

Phase transitions, material ejection, and plume dynamics in pulsed laser ablation of soft biological tissues

Alfred Vogel¹, Ingo Apitz¹, and Vasan Venugopalan²

¹Institut für Biomedizinische Optik, Universität Lübeck
Peter-Monnik-Weg 4, D-23562 Lübeck, Germany

²Dept. of Chemical Engineering and Materials Science and
Laser Microbeam and Medical Program, Beckman Laser Institute
University of California, Irvine, California 92697, USA

1 Introduction

After the invention of the pulsed ruby laser by Maiman in 1960 it was anticipated that lasers would enable the cutting and removal of biological tissue with unprecedented precision and selectivity [1]. However, even though pulsed lasers were used within a few years for intraocular tissue *coagulation*, a clinically viable application of pulsed laser *ablation* was not reported until the early 1970's. It would take until the 1980's for lasers to be routinely used for ophthalmic dissection and ablation procedures [2,3]. In other medical sub-specialties routine laser use did not begin until the mid 1980's. The delay between the invention of the laser and its successful clinical application was largely due to a lack of understanding of the fundamental mechanisms that govern laser–tissue interactions. Now, as we approach the 50th anniversary of the invention of the laser, the understanding of laser–tissue interactions has matured and procedures that employ pulsed laser radiation are not only present in nearly every medical sub-specialty but also in various biological fields.

In the 1990's, two books on laser–tissue interactions became available and serve as a valuable resource for the field [4,5]. However, a comprehensive review of the fundamental mechanisms involved in pulsed laser ablation of tissue appeared only very recently when Vogel and Venugopalan [6] presented a conceptual framework providing mechanistic links between various ablation applications and the underlying thermodynamic and phase change processes. The present article summarizes key elements of this analysis, with focus on the kinetics of rapid phase transitions in aqueous media and their modifications by the presence of a tissue matrix. The results obtained are then used to analyse the mechanisms of material ejection in pulsed laser tissue ablation and their consequences for ablation efficiency, precision, and collateral damage. Description of the ablation plume dynamics will be an essential part of this analysis because the composition of the plume reflects the kinetics of

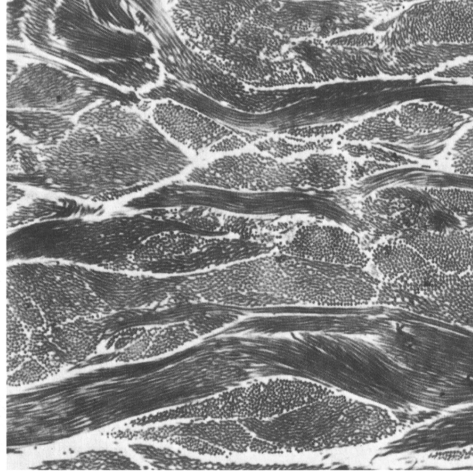


Figure 1. Transmission electron micrograph of human skin (dermis) showing collagen fibres sectioned both longitudinally and transversely. Magnification $4900\times$. The fibres consist of individual fibrils that are embedded in a ground substance with high water content (Reprinted with permission from Ref. [8]. Copyright 1988 Blackwell Science).

the initial phase transitions, and its rapid movement produces a recoil pressure that may result in secondary material ejection. We will confine the presentation to pulsed ablation at tissue surfaces that does not involve plasma formation. Ablation processes within transparent tissues or within cells that involve nonlinear absorption have been considered in recent reviews [6,7].

2 Tissue composition, and properties relevant for ablation

Soft biological tissues consist of cells that reside in and attach to an extracellular matrix (ECM). By mass, the composition of most soft tissues is dominated by water (55-99%) and collagen (0-35%). In “cell-continuous” tissue such as liver and epithelia, the ECM fraction is quite small and consists mostly of cell adhesion proteins. By contrast, “matrix-continuous tissues” that include the corneal stroma, dermis, cartilage, and tendon have a very small cellular fraction and are almost entirely ECM. In matrix-continuous tissues (see Fig. 1), the ECM consists largely of collagen, with the collagen content being as high as 35% [6,9]. A primary ECM function is the maintenance of the tissue’s structural integrity. As a result, the ECM inhibits both tissue vaporization and material removal that represent the desired outcomes of ablation processes.

In general, the *optical absorption properties of tissue* are dominated by the absorption of proteins, DNA, melanin, hemoglobin, and water. The absorption spectra of these tissue constituents are presented in Fig. 2. In non-turbid samples, optical

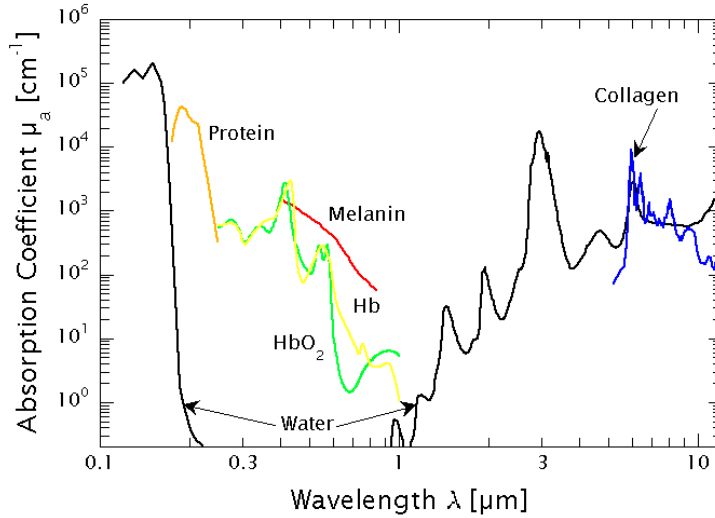


Figure 2. Optical absorption coefficients of principal tissue chromophores in the 0.1–12 μm spectral region. (Reprinted with permission from Ref. [6]. Copyright 2003 American Chemical Society)

transmission T is governed by Beer-Lambert's law according to:

$$T = \left[\frac{\Phi}{\Phi_0(1 - R_s)} \right] = \exp(-\mu_a l), \quad (1)$$

where R_s is the specular reflection of the sample and Φ is the radiant exposure transmitted after travel through an optical path length l in a sample with absorption coefficient μ_a [cm^{-1}]. In the absence of scattering, the reciprocal of the absorption coefficient ($1/\mu_a$) defines the optical penetration depth δ and thus the characteristic depth of laser energy deposition.

For most laser wavelengths used only a single tissue constituent (e.g., water or collagen) absorbs the radiation. Therefore the spatial scales that characterize the distribution of these constituents are vital to understanding the potential energy transfer mechanisms between tissue constituents. The vast majority of tissue water resides in cells and in the ground substance of the ECM in which the collagen fibrils are embedded [6,10], and the spatial scale characterizing domains with different absorption properties is given by the diameter and spacing of the collagen fibrils. The fibril diameter is ≈ 30 nm in cornea and varies between 20 nm and 120 nm in dermis. The centre-to-centre spacing is very regular (≈ 65 nm) in the transparent cornea and exhibits more variations in other tissues [6,9].

Optical scattering arises from spatial variations in refractive index within tissue that are particularly strong between collagen fibrils and ground substance. Typical reduced scattering coefficients for tissues in the green are on the order of $\mu'_s = 10$ – 40 cm^{-1} [11]. The wavelength dependence of the reduced scattering coefficient μ'_s is

well characterized by the scaling law $\mu'_s \sim \lambda^{-b}$ where $b \sim 0.5-2$ [12,13]. Optical scattering will reduce the optical penetration depth δ of light relative to the absorption depth ($1/\mu_a$). In addition, when scattering is dominant over absorption, backscattering and total internal reflection lead to a fluence rate proximal to the tissue surface that can exceed by several times the incident irradiance [14,15]. However, ablation is typically performed at wavelengths where $\mu_a \gg \mu'_s$.

The thermal and mechanical transients generated during the pulsed laser ablation process are substantial and can result in *dynamic changes of the optical absorption properties*. Motivated by spectroscopy literature indicating that the absorption peak of water at $\lambda = 2.94 \mu\text{m}$ drops and shifts towards shorter wavelengths for increasing temperature [18], various researchers investigated the reduction in the IR absorption coefficient of tissue when heated [16,19,20]. In Fig. 3 we present data for the dependence of the absorption coefficient of water on volumetric energy ε for $\lambda = 2.94$ and $2.79 \mu\text{m}$ [16,17], and of the variation in optical penetration depth with incident radiant exposure [6]. The latter results, shown in the bottom of Fig. 3, demonstrate that for $\Phi_0 > 0.5 \text{ J/cm}^2$, Er:YSGG laser radiation ($\lambda = 2.79 \mu\text{m}$) offers better spatial confinement of the laser energy compared to Er:YAG laser radiation ($\lambda = 2.94 \mu\text{m}$). This is opposite to the behaviour one would expect from the absorption coefficients measured at small radiant exposures (Fig. 2). Variations in optical absorption with temperature are also important for ultraviolet laser ablation. Staveteig and Walsh [21] hypothesized that absorption of UV radiation by peptide bonds is followed by heating of the surrounding water that results in a change in hydrogen bonding structure of water and thus to a red shift of the water absorption band, which at room temperature is located at 160 nm. They demonstrated that the absorption of water at $\lambda = 193 \text{ nm}$ may be raised to as much as $\mu_a \approx 10^4 \text{ cm}^{-1}$ at $\varepsilon = 2 \text{ kJ/cm}^3$.

Phase transitions of the tissue water are strongly influenced by the *mechanical tissue properties*. There is a positive correlation between tissue strength and collagen content. Tissues that represent extremes of mechanical strength are the liver and tendon. Liver is a cell-continuous tissue with little ECM and collagen content, which results in a very low ultimate tensile strength (UTS) of 23 kPa and moderate extensibility at fracture $\sim 50\%$ [9,22]. Tendon is a matrix-continuous tissue that possesses high collagen content. This provides for high strength and stiffness with an UTS of $\gtrsim 100 \text{ MPa}$ and fracture extensibility of $\sim 10\%$. Skin has similarly high collagen content (25–33%) but lower UTS ($\sim 10 \text{ MPa}$) and much larger fracture extensibility of $\sim 30-100\%$ because the collagen fibrils in the dermis are “wavy” and form a loose three-dimensional network [9] (see Fig. 1).

Nearly all tissue mechanical data have been acquired under “quasi-static” loading conditions in which the tissue is deformed at very slow strain rates; typically on the order of 10^{-3} s^{-1} . However, the processes involved in pulsed laser ablation of tissue produce extremely high strain rates; on the order of 10^5-10^7 s^{-1} . Studies performed to examine the effect of strain rate in the range $0.3-170 \text{ s}^{-1}$ have revealed that while the tissue strain at fracture remains roughly constant, the UTS increases in proportion to the logarithm of the strain rate [23–25]. The increase in UTS is due to the viscous dissipation between the collagen fibrils and the adjacent ground substance during the rapid deformation. It is not known whether the logarithmic dependence between strain rate and tissue UTS remains valid at the extreme strain

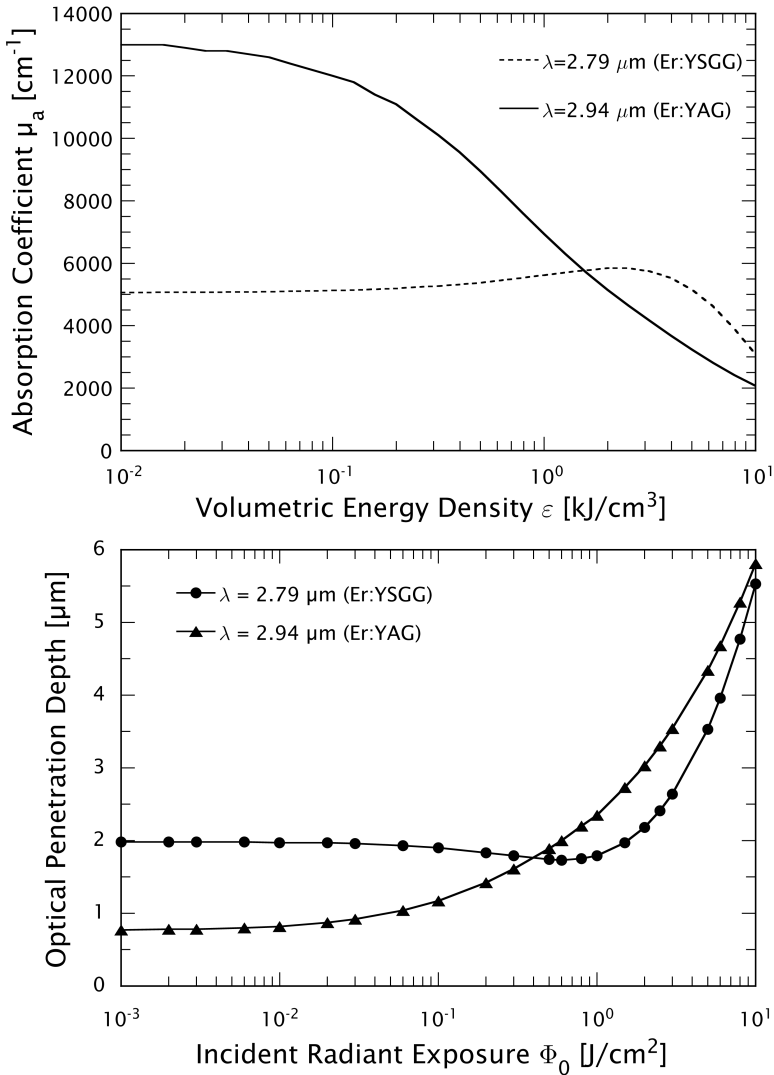


Figure 3. Graphs illustrating the effects of dynamic optical properties of a water target produced by Er:YAG ($\lambda = 2.94 \mu\text{m}$) and Er:YSGG ($\lambda = 2.79 \mu\text{m}$) laser irradiation; top: variation of optical absorption coefficient of water with volumetric energy density. Data compiled from Refs. [16] and [17]; bottom: variation of optical penetration depth with incident radiant exposure. Optical penetration depth is defined as the location at which the volumetric energy density drops to $1/e$ of the surface value. Note that for incident radiant exposures $F_0 > 0.4 \text{ J}/\text{cm}^2$, Er:YSGG laser irradiation offers more superficial energy deposition compared to Er:YAG laser irradiation.

rates produced by pulsed laser ablation. However, the available UTS data suggest that the tissue strength under ablative conditions can be considerably higher than

that measured under “quasi-static” loading conditions.

Thermal denaturation of collagen fibrils can affect the dynamics of the ablation process. It begins when the thermal energy of the constituent molecules overcomes the weak hydrogen bonds and van der Waals interactions stabilizing the helical configuration of the α -chains in the collagen molecule [26]. The “native” triple-helical structure of the molecule is thus transformed into a “denatured” random coil structure that is associated with a loss of the banding pattern of the native collagen fibrils in TEM [27] and with shrinkage of the fibrils along their longitudinal axis [28]. However, when the collagen is embedded in tissue, shrinkage is impaired and tensile stress is developed along the fibrils due to the covalent cross-links that connect the molecules and maintain the organization of the fibrils [29,30]. Further heating denatures first the thermally-labile and then the thermally-stable covalent cross-links between the collagen molecules. This results in a stepwise disintegration of the collagen fibrils [31], a relaxation of the stresses developed during shrinkage [29,30], and finally in total mechanical failure of the fibrillar tissue structure that now appears homogeneous in TEM [26,27]. Older tissues possess a higher density of cross-links and thus require higher temperatures to undergo these transitions [28,32].

Thermal denaturation is a rate process and thus depends on both the magnitude and duration of thermal exposure [33,34]. If the heating time is reduced, considerably higher temperatures are required for denaturation. While the mechanical stability of collagen is destroyed at about 75°C when heated for several minutes [29], temperatures far in excess of 100°C are required to affect mechanical stability for thermal exposures in the nanosecond to microsecond range characteristic of pulsed laser ablation [35]. Nevertheless, given that surface temperatures approaching 400–750°C have been measured during tissue ablation using laser pulses of 100 μ s duration [36], the mechanical integrity of the tissue ECM will certainly be compromised. In nanosecond ablation, temperatures in the superficial tissue layer may, even at moderate radiant exposures, be raised above 1000°C at which point the mechanical integrity of the tissue ECM is completely lost due to thermal dissociation of the constituent molecules into volatile fragments [37] (see Sect. 4.6).

Laser wavelengths especially useful for precise tissue ablation are those that exhibit very large absorption coefficients (see Fig. 2) such as the radiation of ArF excimer lasers ($\lambda = 193$ nm), Er:YSSG lasers ($\lambda = 2.79$ μ m), Er:YAG lasers ($\lambda = 2.94$ μ m), and CO₂ lasers ($\lambda = 10.6$ μ m). Since these wavelengths cannot well be transmitted through optical fibres, they are mainly used for ablation at tissue surfaces in air. For ablation inside the human body, XeCl excimer lasers ($\lambda = 308$ nm), thulium:YAG lasers ($\lambda = 2.0$ μ m) and holmium:YAG lasers ($\lambda = 2.1$ μ m) are frequently employed because their radiation is transmitted by low-OH quartz fibres.

3 Linear thermo-mechanical response to pulsed irradiation

In the absence of photochemical processes, the laser energy absorbed by the tissue is completely converted to a *temperature rise* before a phase transition occurs. Under adiabatic conditions, the temperature rise at a location r is related to the local

volumetric energy density $\varepsilon(r)$ by:

$$\Delta T(r) = \frac{\varepsilon(r)}{\rho c_v}, \tag{2}$$

where ρ is the tissue density and c_v the specific heat capacity at constant volume. The absorbed energy is redistributed by thermal diffusion [38]. In 1983, Anderson and Parrish [39] introduced the concept that spatially-confined microsurgical effects can be achieved by using laser pulse durations t_p shorter than the characteristic thermal diffusion time of the heated volume. For laser ablation, the heated volume is typically a layer with a thickness of the optical penetration depth ($1/\mu_a$), and the characteristic thermal diffusion time t_d is given as [14]

$$t_d = \frac{1}{\kappa \mu_a^2}, \tag{3}$$

where κ is the thermal diffusivity. By defining a dimensionless ratio $t_d^* = (t_p/t_d)$, the thermal confinement condition can be expressed as [40,41]

$$t_d^* = \frac{t_p}{t_d} = \kappa \mu_a^2 t_p \lesssim 1. \tag{4}$$

Short-pulse laser irradiation of tissue not only leads to rapid heating but also to the *generation and propagation of thermoelastic stresses* [42]. The magnitude and temporal structure of these stresses are governed by the longitudinal speed of sound in the medium c_a , the laser pulse duration t_p , the depth of the heated volume ($1/\mu_a$) and the Grüneisen coefficient Γ [42,43]. The Grüneisen coefficient is simply the internal stress per unit energy density generated when depositing energy into a target under constant volume (i.e., isochoric) conditions. This is given by the thermodynamic derivative

$$\Gamma = \left(\frac{\partial \sigma}{\partial \varepsilon} \right)_v = \frac{\beta}{\rho c_v \kappa_T}, \tag{5}$$

where σ is the internal stress, ε the volumetric energy density, v the specific volume, β the coefficient of thermal expansion, ρ the mass density, c_v the specific heat capacity at constant volume and κ_T the isothermal compressibility.

Thermoelastic stresses are most prominent when the laser pulse duration t_p is smaller than the characteristic time required for a stress wave to traverse the heated volume $t_m = (1/\mu_a c_a)$ [14]. This means that the stresses are confined within the heated region during the laser irradiation. By defining a dimensionless ratio $t_m^* = (t_p/t_m)$, the “stress confinement” condition can be expressed as [40,41]

$$t_m^* = \frac{t_p}{t_m} = \mu_a c_a t_p \lesssim 1. \tag{6}$$

For $t_m^* \ll 1$, heating of the laser-affected volume occurs under isochoric conditions and the thermoelastic stress is maximal. The peak stress σ_p is given by [42]

$$\sigma_p = A\Gamma\varepsilon_0 = A\Gamma\mu_a\Phi_0, \tag{7}$$

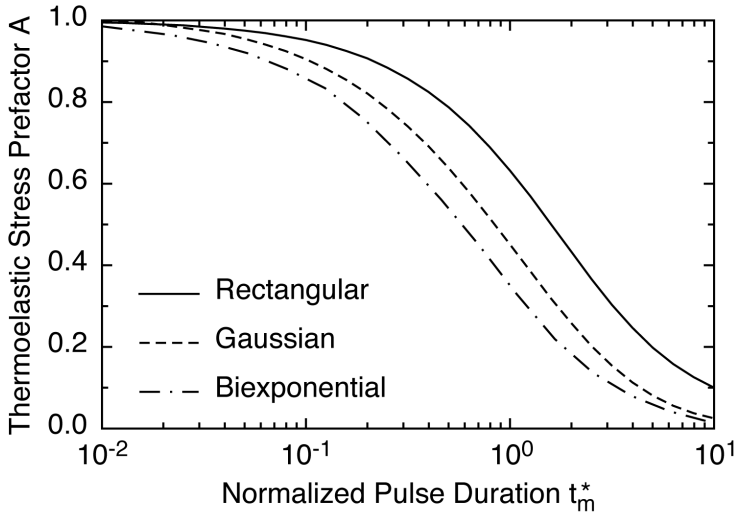


Figure 4. Variation of the thermoelastic stress prefactor A (see Eq. (7)) with pulse duration relative to the stress propagation time across the heated volume t_m^* . Results are shown for a rectangular, biexponential, and Gaussian laser pulse shape and derived from the results of Refs. [42] and [44].

where $A = 1$ and the duration of the thermoelastic stress transient t_a scales with the stress propagation time and $t_a \approx (4-6/\mu_a c_a)$. When the stress transient leaves the heated volume, the peak stress drops to $0.5 \sigma_p$.

In the limit $t_m^* \rightarrow \infty$, where there is no stress confinement, $A \rightarrow 0$ and the duration of the stress transient approaches that of the laser pulse. The variation of A with t_m^* for different temporal laser pulse shapes is shown in Fig. 4.

While thermal expansion of a heated volume generates compressive thermoelastic stresses, subsequent propagation of these stresses results in transients that contain both compressive and tensile components. Tensile stresses arise from the reflection of the compressive stress waves at a boundary to a medium with lower acoustic impedance (tissue–air, tissue–water) or from the three-dimensional characteristics of acoustic wave propagation from a heated tissue volume of finite size [7,43,45–48]. Tensile stress wave generation originating from acoustic impedance mismatch at a tissue surface is shown in Fig. 5.

4 Thermodynamics and kinetics of phase transitions

All ablation processes involve the fracture of chemical bonds and lead to the removal of single molecules, molecular fragments, and molecular clusters. Bond fracture can also produce the formation of voids (i. e., bubbles or cracks) that facilitate the ejection of non-decomposed material fragments upon mechanical failure of the target. Vaporization, molecular fragmentation, and void formation can all be viewed as phase transitions that are accomplished via photothermal, photomechanical, and/or pho-

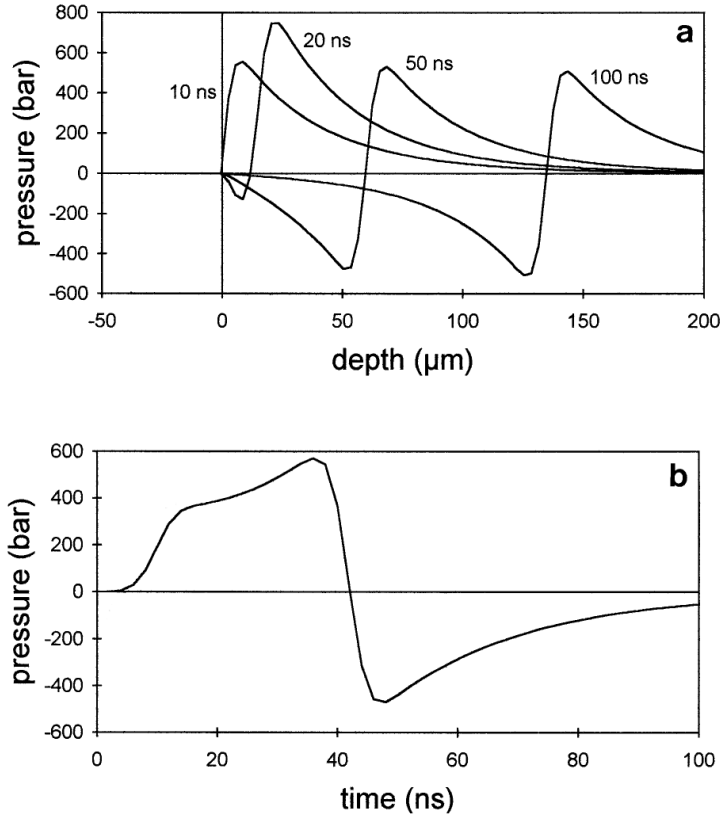


Figure 5. (a) Development of a thermoelastic stress wave in water calculated for $F_0 = 2 \text{ J/cm}^2$; $\mu_a = 200 \text{ cm}^{-1}$ and $t_p = 8 \text{ ns}$. (b) Pressure as a function of time at a depth of $50 \mu\text{m}$. (Reprinted with permission from Ref. [45]. Copyright 1996 Springer).

tochemical mechanisms. In this article, we focus on the kinetics of phase transitions in purely photothermal ablation processes such as in IR ablation. When UV lasers are used, photochemical bond dissociation may contribute to ablation. For a detailed discussion of the role of these photochemical processes, the reader is referred to a recent review by two of the authors [6].

4.1 Phase diagrams

We use the pressure vs. temperature projection of the phase diagram for liquid and gaseous water (Fig. 6) and the pressure vs. specific volume projection of the thermodynamic phase diagram (Fig. 7) to discuss the thermodynamics of phase transitions. The solid curve $A-C$ on Fig. 6 represents those pressure/temperature pairs where liquid and gaseous water are in equilibrium with each other and is known as the “binodal”. The curve $B-C-D$, the “spinodal”, denotes a locus of states with infinite

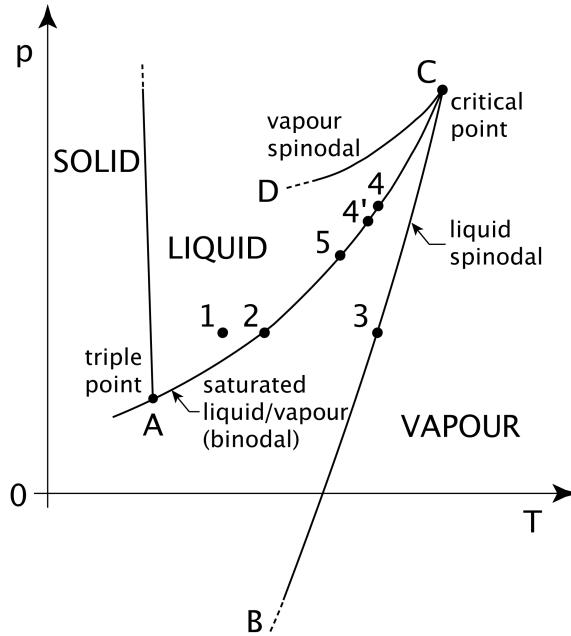


Figure 6. Pressure vs. temperature projection of the thermodynamic phase diagram including the spinodal curve. Specific states of interest are (1) ambient temperature and pressure, (2) boiling temperature under ambient conditions, (3) spinodal temperature at ambient pressure, (4) saturated conditions corresponding to the ambient spinodal temperature. The importance of points 4' and 5 are discussed in Sect. 5.4.

compressibility representing the intrinsic stability limit of the liquid or vapour phase [$(\partial T/\partial s)_p = 0$ and $(\partial p/\partial v)_T = 0$]. At the spinodal, the superheated liquid phase ($B-C$) or subcooled vapour ($C-D$) phase is no longer stable with respect to the random density fluctuations that are present in all materials at non-zero temperatures. The region between segment $A-C$ of the binodal and $B-C$ of the spinodal represents metastable states of the superheated liquid for which the presence of a free surface or bubble nucleus is required for vaporization. The binodal and spinodal curves intersect at the critical point C above which no thermodynamic distinction can be made between liquid and vapour phases. For water, the critical point is located at $T_c = 374.14^\circ\text{C}$ and $p_c = 22.09\text{ MPa}$.

Liquid, vapour, and mixed phase regions are clearly demarcated in the $p-v$ diagram of Fig. 7. The binodal encompasses the mixed phase region that specifies the range of specific volumes in which liquid and gaseous phases coexist for a given pressure and temperature. The dashed curve provides the spinodal where the segment $B-C$ represents the stability limit of superheated liquid and segment $C-D$ represents the stability limit of subcooled vapour.

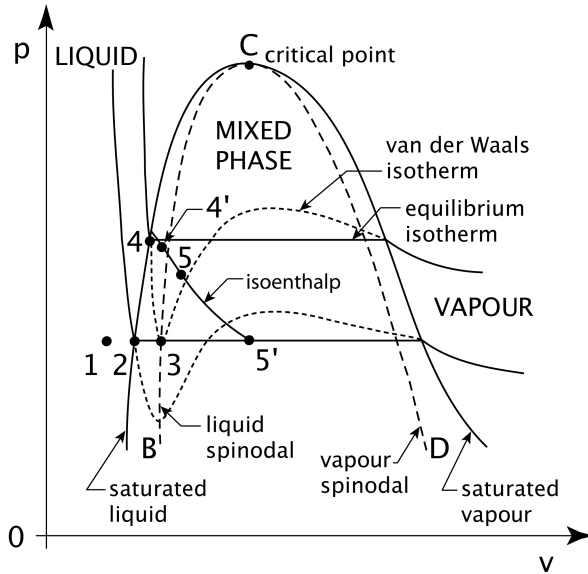


Figure 7. Pressure vs. specific volume projection of the thermodynamic phase diagram including the spinodal curve and equilibrium and van der Waals isotherms. Points 1–4 correspond to those shown in Fig. 11. The importance of points 4', 5, 5' and the isoenthalp is discussed in Sect. 5.4.

4.2 Surface vaporization

Equilibrium vaporization at a liquid–vapour interface is associated with an increase of specific volume at constant temperature that requires the latent heat of vaporization. This process can occur at any single location along the binodal in the p – T diagram of Fig. 6. In the p – v diagram in Fig. 7, surface vaporization is represented by a path following an equilibrium isotherm that connects a state of saturated liquid with a state of saturated vapour. Thus vaporization does not occur at a pre-determined temperature and theoretical models that adopt a fixed “vaporization temperature” [49] violate the basic physics of the process [50]. The actual surface temperature is dictated by the rate of equilibrium vaporization that balances the irradiance supplied to the system.

However, during laser ablation, rates of vapour formation in excess of that predicted by equilibrium vaporization are often achieved. This occurs because the increased equilibrium vapour pressure corresponding to the increased temperature of the liquid surface is not established instantaneously. This results in an increased mass flux of vapour transported into the surroundings known as non-equilibrium interphase mass transfer and can be estimated using arguments from the kinetic theory of gases [51,52]. Nevertheless, even this increased non-equilibrium interphase mass transfer provides a very small ablation rate. *Efficient* ablation is achieved at laser irradiances that deposit energy at a rate that cannot be balanced by surface vaporization processes alone. This results in material removal via *volumetric* processes.

4.3 Normal boiling

Normal boiling refers to a volumetric process that forms vapour at a thermodynamic state on the binodal as indicated by point 2 in Fig. 6. Thus, for a given pressure, the binodal defines the corresponding “boiling temperature”. For water at atmospheric pressure this temperature is 100°C. However for ablation processes with a high rate of mass removal, the boiling temperature is increased significantly because the recoil produces an increase in pressure both at the target surface and within its bulk.

Vapour formation in normal boiling relies on the presence of pre-existing nuclei of vapour or dissolved gas within the liquid to catalyze the nucleation and growth of vapour bubbles. The transition from saturated liquid to saturated vapour occurs within a finite layer of mixed phase. The thickness of this “vapour–liquid” layer is comparable to the optical penetration depth of the incident radiation and its composition varies from that of saturated liquid at its base to saturated vapour at the target surface [50,53]. As a result, the surface temperature is fixed at the saturation conditions corresponding to the pressure at the target surface and there is no temperature gradient within the vapour–liquid layer.

It is important to note that once a normal boiling process is established, the presence of volumetric energy densities corresponding to temperatures slightly higher than the saturation temperature results in the growth of vapour bubbles. Therefore normal boiling processes always involve *partial vaporization* of a liquid volume through the growth of vapour bubbles. Thus the concept frequently found in biomedical ablation papers that vaporization only occurs once the entire latent heat of vaporization is deposited is not correct.

Nevertheless, normal boiling plays a negligible role for pulsed laser ablation for two reasons. First, the density of heterogeneous bubble nucleation sites is likely insufficient to provide a boiling process sufficiently vigorous to balance the high rates of energy deposition achieved in most pulsed laser ablation processes [41,50]. Second, the high rates of energy deposition can be balanced only if the bubbles move to the target surface on a time scale set by the propagation velocity of the ablation front. Miotello and Kelly [54] showed that this is not possible when irradiating pure water with nanosecond laser pulses and is possible for microsecond pulses only for radiant exposures proximal to the ablation threshold. In tissue this is even less likely because the mobility of vapour bubbles is further inhibited by the presence of the ECM.

4.4 Phase explosion and explosive boiling

When the rate of volumetric energy deposition provided by laser radiation is more rapid than the rate of energy consumed by vaporization and normal boiling, the tissue water is driven to a metastable superheated state. The superheated liquid is metastable until the spinodal temperature is reached. The spinodal limit is defined by line *B–C* in Fig. 6 that represents the locus of states with infinite compressibility $[(\partial p/\partial v)_T = 0]$. At the spinodal limit, the superheated liquid undergoes “spinodal decomposition”; a spontaneous process by which a thermodynamically unstable liquid relaxes towards equilibrium by “phase separation” into a mixture of saturated vapour and saturated liquid [55–57]. The spinodal temperature of water at atmo-

spheric pressure is $\approx 305^\circ\text{C}$ with the corresponding equilibrium saturation vapour pressure of 9.2 MPa. Thus spinodal decomposition under atmospheric conditions involves an impressive pressure rise resulting in the violent emission of saturated liquid droplets by the expanding vapour.

For the phase diagram shown in Fig. 6, the heating phase corresponds to the path $1 \rightarrow 3$, and the spinodal decomposition will initially result in a nearly isochoric transition from point 3 on the spinodal to point $4'$ in the mixed phase region possessing the same enthalpy. For pure water, the subsequent explosive expansion of this mixture will transition through a series of thermodynamic states that follows the curve of constant enthalpy (isoenthalp) as shown in Fig. 7 until the mixture reaches atmospheric pressure at point $5'$. During the expansion $4' \rightarrow 5'$, the temperature of the mixture drops to 100°C , and about half of the liquid is transformed into vapour. The vapour fraction ($\sim 49.6\%$) is given by the energy density necessary to heat water from room temperature to the spinodal limit (1.27 kJ/g) as compared to the sum of the sensible and latent enthalpy of vaporization. The remaining saturated liquid is ejected in the form of droplets.

To provide a complete description of the phase transformation process as the liquid is heated to the spinodal limit, one must also consider the potential contribution of homogeneous nucleation [41,54,58,59]. Homogeneous nucleation refers to the spontaneous formation of vapour inclusions within the bulk liquid that arise solely from thermodynamic fluctuations and is not catalyzed by the presence of impurities or dissolved gas. While the formation of such vapour “nuclei” is spontaneous, their growth is not ensured and depends strongly on superheat temperature.

In classical nucleation theory, the driving force for growth of vapour nuclei is supplied by the difference in chemical potential between the superheated liquid outside the bubble and the vapour inside the bubble. This driving force is necessary to overcome the free energy barrier posed by the surface tension separating the vapour from the liquid [57]. The chemical potential difference between the superheated liquid and vapour scales with the bubble volume (i. e., r^3) while the contribution from surface tension scales with the bubble surface area (i. e., r^2). As a result, small vapour nuclei that form due to thermodynamic fluctuations spontaneously collapse while larger vapour nuclei will grow. The Gibbs free energy ΔG that describes the thermodynamics of bubble formation is given by:

$$\Delta G = \frac{4\pi r^3}{3}(\mu_v - \mu_l) + 4\pi r^2\sigma, \quad (8)$$

where μ_v and μ_l are the chemical potentials of the vapour and liquid state, respectively, r is the size of the vapour nuclei, and σ is the surface tension of the surrounding liquid [57,60]. Nuclei grow if they are larger than a critical radius r_{cr} . Figure 8 shows the dependence of r_{cr} on superheat temperature for water. Note that while r_{cr} strongly decreases as the superheat temperature increases, it remains finite even at the spinodal temperature. Thus nucleation remains an activated process with a finite free energy barrier [55]. The strong reduction of Δr_{cr} results in a dramatic rise in the nucleation rate J with temperature that attains a large, but finite, value at the spinodal temperature as shown in Fig. 9. The energy barrier that must be overcome for the conversion from the liquid to vapour phase disappears only when surface

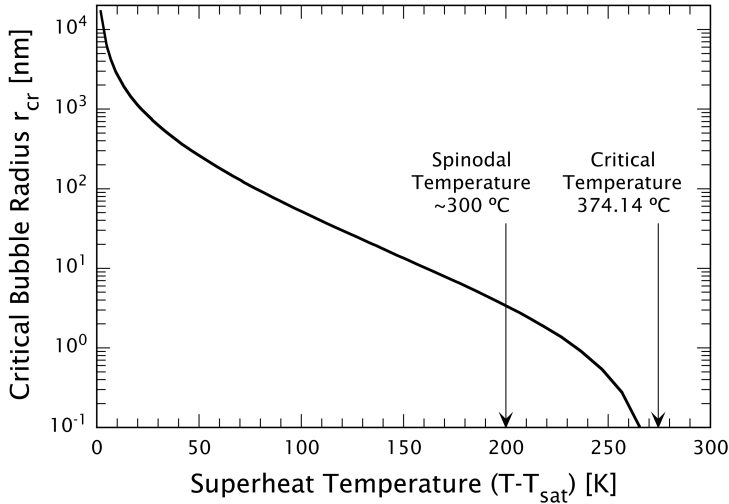


Figure 8. Variation of the critical bubble radius required for spontaneous vapour bubble growth with superheat temperature. Note that the critical bubble radius goes to zero at the critical temperature.

tension disappears and this occurs at the critical point. To account for the influence of statistical fluctuations on the stability limit, Kiselev has introduced the concept of a *kinetic spinodal*. The kinetic spinodal is defined as the locus of thermodynamic states where the time for spontaneous formation (driven by superheat temperature) of vapour nuclei becomes smaller than the characteristic time for their decay to local equilibrium (driven by surface tension) [61]. The superheat temperatures defined by the kinetic spinodal are much lower than the critical temperature and slightly lower than the classical spinodal and represent the physical limits of the metastable liquid states that can be achieved prior to spinodal decomposition.

Thus, in general, the transformation of superheated (metastable) liquid to an equilibrium state of mixed phase may involve both bubble nucleation (large density fluctuations extending over a small spatial extent) and spinodal decomposition (small density fluctuations extending over a large spatial extent). We refer to the collective phase transition process as a *phase explosion*. A more detailed consideration of nucleation theory and spinodal decomposition as it relates phase transitions and tissue ablation can be found in our earlier review [6].

Thus far we have focused on processes tracing a path indicated by $1 \rightarrow 3 \rightarrow 4' \rightarrow 5 \rightarrow 5'$ in Figs. 6 and 7. This path corresponds to the extreme case in which no vapour nuclei are present in the liquid. When the heating occurs very rapidly at high radiant exposures, the liquid experiences a recoil pressure from surface vaporization/interphase mass transfer that can be substantial due to the non-equilibrium conditions produced during the beginning of the laser pulse. Thus spinodal conditions are reached at an elevated pressure somewhere between point 3 and the critical point C . Because the resulting phase explosion occurs at elevated temperature and

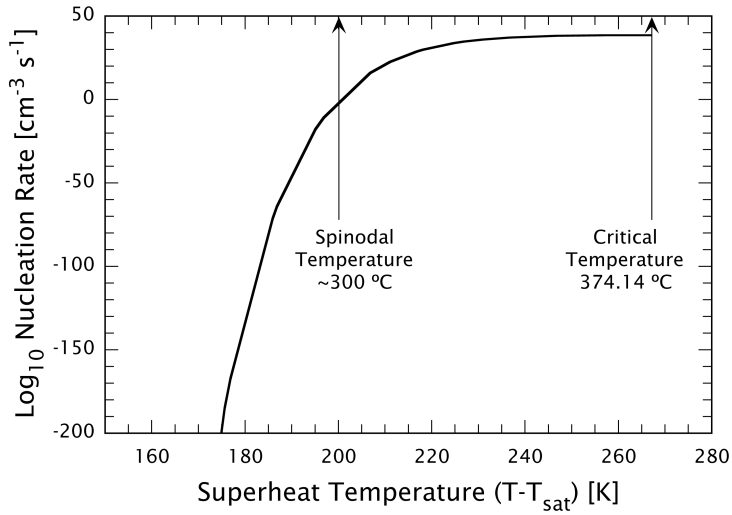


Figure 9. Variation of vapour bubble nucleation rate with superheat temperature.

pressure, the pressure jump associated with the phase separation is less severe. The elevated temperature corresponds to a higher volumetric energy density of the superheated liquid, and therefore more than half of the liquid will be transformed into vapour during the phase separation process.

When vapour nuclei are present in the liquid and the heating occurs on a time scale such that a significant fraction of the incident laser energy (but not the entire energy flux) contributes to the growth of heterogeneous and homogeneous vapour nuclei, the resulting phase transition process again follows a path that is intermediate between normal boiling and the path $1 \rightarrow 3 \rightarrow 4$. Spinodal conditions in the superheated liquid are again reached at a location between point 3 and the critical point C followed by phase separation. In this case however, the pressure rise is due to vapour formation at the nucleating centres rather than recoil from vapour leaving the target surface. Such intermediate processes are termed “*explosive boiling*”. In general, the energy necessary to reach spinodal conditions is higher for explosive boiling than for the case of phase explosion with surface vaporization. The amount of vapour formation is greater due to contributions from both the growing nucleation centres and the phase separation.

Both phase explosion and explosive boiling are volumetric processes in which a portion of the target material is ejected in the liquid phase and the latent heat of vaporization is not supplied to the entire ablated mass. As a result, the ablation efficiency (mass removed by a given amount of laser energy) is higher for these processes as compared to surface vaporization and normal boiling where all material is removed in the vapour phase.

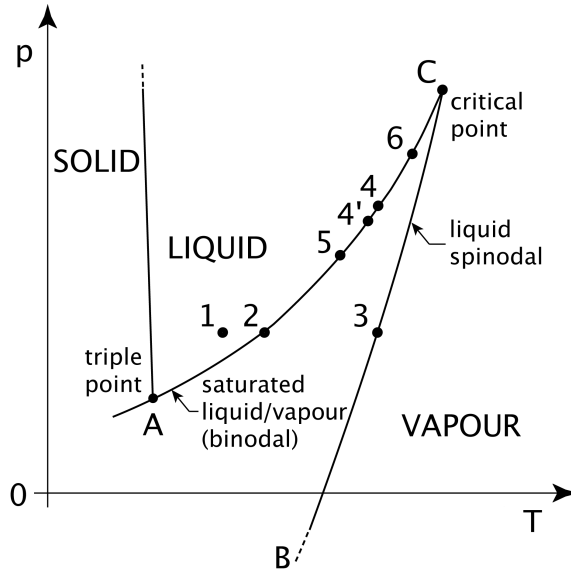


Figure 10. Path taken through the p vs. T projection of the thermodynamic phase diagram for confined boiling ($1 \rightarrow 2 \rightarrow 4 \rightarrow 6$) and for tissue ablation involving a phase explosion ($1 \rightarrow 2 \rightarrow 3 \rightarrow 4' \rightarrow 5 \rightarrow 6$). The actual path followed depends on the rate of energy deposition, number density of heterogeneous nuclei, and the mechanical strength of the tissue matrix relative to the saturation vapour pressure corresponding to the ambient spinodal temperature.

4.5 Effects of the tissue ECM on the phase transitions

In pulsed laser ablation of tissues, the phase transition processes are affected by the presence of the ECM. For boiling processes within tissue, the vapour pressure necessary to drive bubble growth must not only overcome surface tension but also the elastic restoring forces provided by the tissue matrix [62]. Therefore, bubble growth in tissue requires a higher internal pressure than in pure liquids, and the elevated pressure is coupled to an increase in the boiling (saturation) temperature. The pressure increase that develops during the boiling process continues until it exceeds the ultimate tensile strength of the ECM and results in explosive tissue ablation [62]. We term this process “confined boiling”. On the p - T phase diagram in Fig. 10, the confined boiling process corresponds to a path $1 \rightarrow 2 \rightarrow 6$, where the $2 \rightarrow 6$ transition is coincident with the binodal and terminates where the saturated vapour pressure equals the ultimate tensile strength of the tissue. In the presence of a tissue matrix, explosive material ejection will thus occur regardless of the rate of energy deposition. Thus, it is not surprising that explosive material ejection due to confined boiling has also been reported to occur in ablation using continuous irradiation at relatively low irradiances [63,64].

In the above scenario, little vaporization occurs prior to the onset of ablation because bubble growth is impeded by the necessity to deform the tissue matrix. For

mechanically weak tissues, much of the ejected mass consists of tissue that is fragmented and accelerated by the phase explosion. In these cases, the ablation enthalpy can thus be considerably smaller than the vaporization enthalpy of water. However, for tissues that possess a strong ECM (e. g., skin), temperatures of 400°C to 700°C are required to produce a saturation vapour pressure exceeding the ultimate tensile strength to initiate ablation [36]. Under these conditions, the ablation enthalpy often exceeds the vaporization enthalpy of water.

The tissue matrix retains its mechanical integrity during nanosecond or microsecond laser exposures even for temperature rises of several hundred degrees. There are several factors that are responsible for this. First, as discussed in Sect. 2, the temperatures required for disintegration of the matrix increase strongly as the duration of heat exposure decreases. Second, the application of tensile stresses to collagen fibrils stabilizes the helical architecture and results in a significant increase of the denaturation temperature. Thus the generation of tensile stresses resulting from pulsed laser heating is expected to further stabilize a collagen ECM with respect to possible collagen denaturation. Third, as discussed in Sect. 2, the extreme strain rates produced by pulsed laser ablation processes ($\sim 10^5\text{--}10^7\text{ s}^{-1}$) likely increase the UTS of the tissue matrix. Thus ablation does not involve a “liquefaction” of the tissue as assumed in earlier models [65,66] but proceeds via the ejection of tissue fragments driven by the vaporization of tissue water.

For low rates of volumetric energy deposition ($\mu_a I$) and high number densities of heterogeneous nuclei, the nature of the ablation process is largely independent of tissue mechanical properties. The laser irradiation will initially heat the tissue under equilibrium conditions at constant pressure ($1 \rightarrow 2$) and then continue on the binodal until the ultimate tensile strength of the tissue is reached, resulting in explosive material removal. However, if the tissue is heated rapidly and/or a small number density of heterogeneous nuclei are present, the tissue water will be driven into a metastable state and a phase explosion will be induced when the spinodal limit is reached ($1 \rightarrow 2 \rightarrow 3 \rightarrow 4' \rightarrow 5$). The subsequent evolution of the process now depends on the mechanical properties of the tissue. Immediate material ejection will result for tissues that are unable to withstand the stresses and deformations associated with the phase explosion. However, tissues possessing high collagen content, and thus high UTS, will not fail mechanically due to the phase explosion. The laser irradiation will then drive a confined boiling process as indicated by path ($5 \rightarrow 6$) in Fig. 10 until the tissue ruptures at higher vapour pressures resulting in material removal. For pulsed ablation of skin, surface temperatures of 400–750 °C have been measured [36], indicating that the dynamic tensile strength of the tissue matrix is higher than the pressure at the critical point ($p_c = 22.09\text{ MPa}$).

4.6 Vapour explosion and photothermal dissociation of the tissue ECM

For ablation using nanosecond pulses, the volumetric energy densities achieved in the tissue water usually exceed the vaporization enthalpy of water [37,41]. Under these conditions, the liquid water is completely transformed into vapour in a process termed “vapour explosion”. Moreover, at temperatures exceeding $\sim 1000^\circ\text{C}$ the constituent molecules of the ECM are thermally dissociated into volatile fragments. Energetically,

these processes result in an ablation enthalpy higher than the vaporization of water and are “less efficient” than phase explosion or confined boiling because they do not involve the ejection of condensed material.

An important factor contributing to the high volumetric energy densities achieved in nanosecond laser ablation is the recoil pressure produced by the ablation of superficial layers of the target. At the beginning of laser exposure, ablation is governed by non-equilibrium surface vaporization (Sect. 4.2). During this phase the recoil pressure is relatively small and a phase explosion occurs as soon as the temperature reaches the spinodal limit (Sect. 4.4). With the onset of the phase explosion, the ablation has transformed from a surface-mediated to a volumetric process resulting in a rapid increase of the recoil stress. This large compressive stress inhibits the ablation of deeper tissue layers until the volumetric energy density is sufficiently high to cause a phase transition that can overcome these higher pressures. Therefore the phase transition of subsurface tissue layers will be more vigorous than the initial surface vaporization because a larger volumetric energy density is required to initiate the phase change process. This, in turn, produces a higher recoil pressure that impedes ablation in deeper tissue layers until even higher volumetric energy densities are reached. At any given depth, ablation starts as soon as the vapour pressure exceeds the recoil pressure resulting from the explosive removal of more superficial layers. This results in a “positive-feedback” process in which the volumetric energy density and pressure values required for the onset of ablation at deeper tissue layers will continue to increase as long as the laser irradiance is increasing within the laser pulse. After the peak irradiance of the laser pulse has passed, the volumetric energy density and pressure at the target surface will decrease while the ablation front continues to propagate into the target. The ablation process becomes most vigorous shortly after the peak of the laser pulse as that is when the volumetric energy density in the target reaches a maximum value [37]. Since the evolution of thermodynamic states within the target is determined both by the incident laser irradiation and by the recoil produced by the ablation plume, ablation will likely continue well beyond the end of the laser pulse [6,37,67]. When the volumetric energy density in the target drops below the value required for thermal dissociation of the tissue matrix, the ejection of particulate tissue fragments will commence [37,67]. Ablation ceases when the vapour pressure within the tissue falls below the ultimate tensile strength of the tissue matrix that itself is influenced by the local denaturation kinetics (Sect. 5).

4.7 Effect of stress confinement on the ablation process

When performing ablation under conditions of stress confinement, the thermoelastic stresses modify significantly the phase transition processes that drive material removal. As discussed in Sect. 3, the thermoelastic stress wave propagation results in both compressive and tensile components (Fig. 5).

The tensile thermoelastic stress waves can produce material ejection at temperatures less than 100°C in liquids with heterogeneous vapour/cavitation nuclei and in mechanically weak tissues such as liver. This phenomenon has been compared to back surface spallation resulting from high-pressure impact [68] and investigated in several studies [69,70]. Nevertheless, temperatures above 100°C are usually necessary

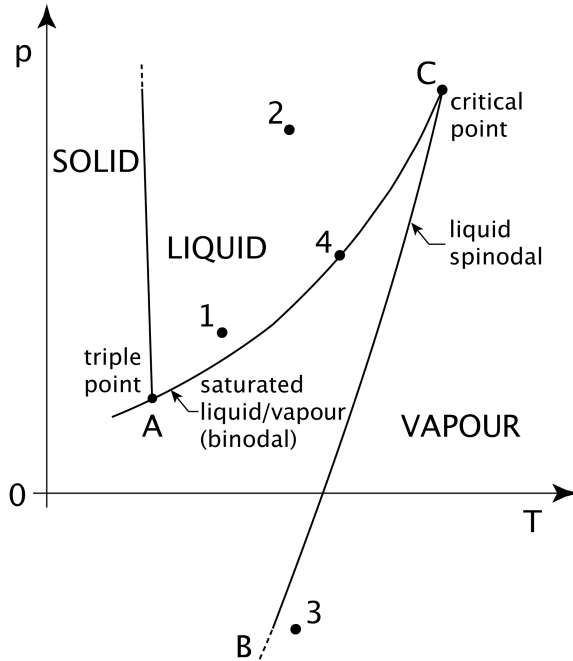


Figure 11. Path taken through the p vs. T projection of the thermodynamic phase diagram for a temperature rise above 100°C under stress confinement conditions. The transition $1 \rightarrow 2$ corresponds to the heating phase that is coupled with the generation of compressive stress. The transition $2 \rightarrow 3$ corresponds to the passage of the tensile stress wave that leads to a crossing of the spinodal limit resulting in phase separation. After the passage of the stress wave, the system reaches point 4 that corresponds to explosive boiling into the large number of bubbles produced shortly before.

to initiate efficient tissue removal [69]. The important influence of tensile stress waves at temperatures above 100°C has only recently attracted attention [6,42]. Figure 11 shows the path taken through the p - T phase diagram for a temperature rise above 100°C produced by laser irradiation with stress confinement. A heating phase ($1 \rightarrow 2$) coupled with the generation of compressive stress is followed by the passage of a tensile stress wave ($2 \rightarrow 3$) that leads to a crossing of the spinodal limit, resulting in a phase explosion. The passage of the stress wave is followed by explosive boiling into the large number of bubbles produced shortly before (point 4) resulting in vigorous material ejection. This ejection occurs at temperatures lower than the spinodal temperature at atmospheric pressure ($T = 305^{\circ}\text{C}$) because, as shown in Fig. 11, the spinodal temperature is reduced with the decrease in pressure provided by the tensile thermoelastic stresses. It is important to note that the sequence of events described above may occur not only during surface ablation in a gaseous environment but also when laser pulses are focussed into a transparent material. They are the basis of the high precision in femtosecond laser nanosurgery of cells [7].

At volumetric energy densities in excess of the spinodal limit at ambient pressure, i. e., for $T > 300^\circ\text{C}$, the superheated liquid is unstable and the onset of explosive ablation need not be initiated by the tensile component of the thermoelastic stress. Nevertheless, the thermoelastic stress transient can still contribute to material removal. The magnitude of thermoelastic transients produced by a given temperature rise under conditions of stress confinement is much larger than the saturation vapour pressure resulting from the same temperature rise and for $T > 1000^\circ\text{C}$ may well exceed 1 GPa. The compressive component of the thermoelastic stress wave upon propagation will develop into a shock wave. The propagation of this shock wave into the depth of the target along with energy dissipation at the shock front [71,72] results in tissue heating at locations beyond those heated directly by the laser irradiation and subsequent heat diffusion. Shock wave propagation thus serves as a form of convective heat transfer that extends the ablation depth and increases ablation efficiency [73]. Experimental evidence for shock wave induced phase changes of water after laser-induced breakdown was provided by Vogel and Noack [74]. For pulsed laser surface ablation, temperatures in the shock wave region will usually be below the spinodal limit since a pressure jump in the neighbourhood of 5 GPa is required to heat water from room temperature to 300°C [71]. Nevertheless, the temperature rise can result in ablation because the tensile component of the thermoelastic stress that follows the shock wave will catalyze an explosive boiling process as described above. Convective heat transfer will become important for ablation only for sufficiently large volumetric energy densities and for very high degrees of stress confinement, i. e. mainly for ultrashort laser pulses. We conclude that regardless of the volumetric energy density, stress confinement invariably serves to lower the ablation threshold and increase ablation efficiency [6,42,69,73,75].

5 Ablation plume dynamics

The phase transitions described in the previous section drive the formation of a plume consisting of material removed from the ablation site. Usually, the ablation dynamics and plume formation is not governed by just a single type of phase transition but by an interplay of different transitions occurring at the target surface and in its bulk. Moreover, the type and strength of the phase transition may change during the laser pulse depending on the volumetric energy densities reached at each target location when the phase change occurs. The characteristics of the ablation plume reflect the underlying ablation dynamics and its analysis provides the insight necessary to draw conclusions about the phase transitions involved in a given ablation event. Furthermore, the plume dynamics influence the ablation process in various ways. The primary ejection of ablation products perpendicular to the tissue surface induces a recoil pressure that may produce additional, secondary material expulsion and cause collateral effects in the bulk tissue. Flow components parallel to the tissue surface that develop at later times may result in a redeposition of ablated material. Scattering and absorption of the incident light by the ablation plume reduce the amount of energy deposited in the target and limit the ablation efficiency at high radiant exposures.

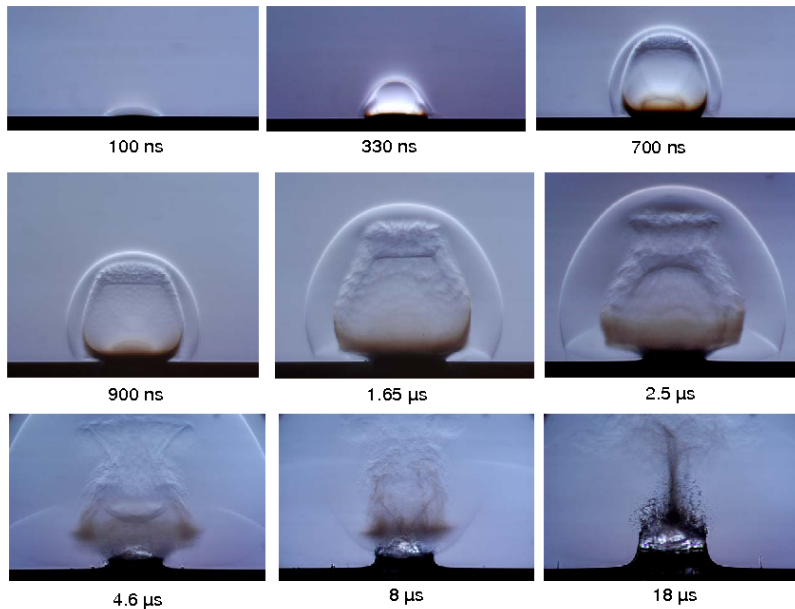


Figure 12. Early phase of water ablation by a Q-switched Er:YAG laser pulse of 70 ns duration, photographed using a novel white light Schlieren technique [76]. The irradiated spot size was $700\ \mu\text{m}$, the radiant exposure $2.8\ \text{J}/\text{cm}^2$ ($25\times$ ablation threshold). All times refer to the beginning of the laser pulse. The dynamics is characterized by vapour plume formation, the emission of external and internal shock waves, droplet ejection, and the onset of recoil-induced material expulsion.

To date, most investigations of the plume dynamics and acoustic phenomena associated with pulsed laser ablation of biological tissues have been performed experimentally by time-resolved photography, probe beam deflectometry, and spectroscopic techniques as reviewed in Refs. [6] and [76]. Here, we focus on the description of the plume dynamics itself rather than on the techniques of investigation. We first discuss the dynamics for water ablation and then progress to the more complicated case of tissue ablation where the primary ablation process and recoil-induced material expulsion are modified by the tissue matrix.

5.1 Primary material ejection in nanosecond ablation

For Q-switched laser pulses of 50–100 ns duration, the rate of energy deposition is extremely large. Close to threshold, the ablation process for liquids such as water is typically characterized by non-equilibrium mass transfer [52] at the target surface followed by a phase explosion of the superficial liquid layer [37]. However, when pulse energies well above the ablation threshold are used, large volumetric energy densities are produced in the target material that result in an ablation process characterized by more vigorous types of phase transitions. To illustrate this, Fig. 12 shows the sequence

of events in the early phase of Q-switched Er:YAG laser ($\lambda = 2.94 \mu\text{m}$) ablation of water for a radiant exposure of 2.8 J/cm^2 , $\approx 25\times$ the ablation threshold. The ablation dynamics is characterized by a succession of explosive vaporization, shock wave emission, and ejection of very fine droplets. The plume remains fairly small until shortly after the peak intensity of the laser pulse, but then rapidly expands. This means that the main part of the ablated material is ejected towards the end and after the laser pulse. The layered structure of the plume reveals that different types of phase transition follow each other while the ablation front propagates into the target. The fact that the top part of the plume is completely transparent indicates that the volumetric energy density in the superficial target layers is larger than the vaporization enthalpy of water at room temperature under atmospheric pressure ($\varepsilon = 2.59 \text{ kJ/cm}^3$). Therefore, this entire liquid volume is transformed into vapour in a “vapour explosion”. When the ablation front has reached a depth where the energy density becomes smaller than the vaporization enthalpy of water, the superheated tissue water starts to decompose into vapour and liquid in a phase explosion, and droplet ejection commences. Droplet ejection is first visible after $\approx 700 \text{ ns}$ and lasts for a few microseconds. The droplets cannot be resolved on the photographs and appear as a reddish haze. The reddish color indicates that the droplet size is sufficiently small to cause Rayleigh scattering by which blue light is scattered much stronger than red light [77]. As a consequence, the red spectral components of the illumination dominate the light that passes through the imaging optics. While the droplet ejection still continues, an indentation of the water surface forms and a “splash” region develops at the periphery of the ablation spot due to the recoil pressure produced by the phase transitions (see Sect. 5.3 below).

When soft tissues are ablated at moderate radiant exposures, the entire ablation plume consists of tissue fragments, as illustrated in Fig. 13(b) for Er:YAG laser ablation of liver at a radiant exposure of 1.4 J/cm^2 . At the same radiant exposure, the top layer of a water target is already completely vaporized and thus transparent as shown in Fig. 13(a). At a larger radiant exposure of 5.4 J/cm^2 (Fig. 13(c)), the top part of the plume becomes transparent for both water and liver ablation, and particulate fragments are ejected only after about 200 ns. The sequence of gaseous ablation products followed by particulates could be visualized only by means of a photographic setup suited for detecting phase objects. In previous studies only the particulate fragments were observed and it was concluded mistakenly that the ablation process commences well after the end of the laser pulse [78]. In reality, the transparency of the top part of the plume indicates that during the initial ablation phase tissue water is completely vaporized and biomolecules are thermally dissociated into volatile fragments, which occurs at temperatures above 1000°C . For the liver target, the subsequent ejection of larger, non-transparent tissue fragments is driven by a phase explosion of the tissue water. The pressure developed during the phase separation suffices to rupture the weak tissue matrix in liver parenchyma (Sect. 4.5). The ejection ceases when the ablation front reaches a depth where the temperature drops below the stability limit of the superheated tissue water. The different optical appearance of the transparent and opaque parts of the ablation plume is due to differences in molecular composition and particle size distribution but not necessarily indicative for disparities in the average mass density.

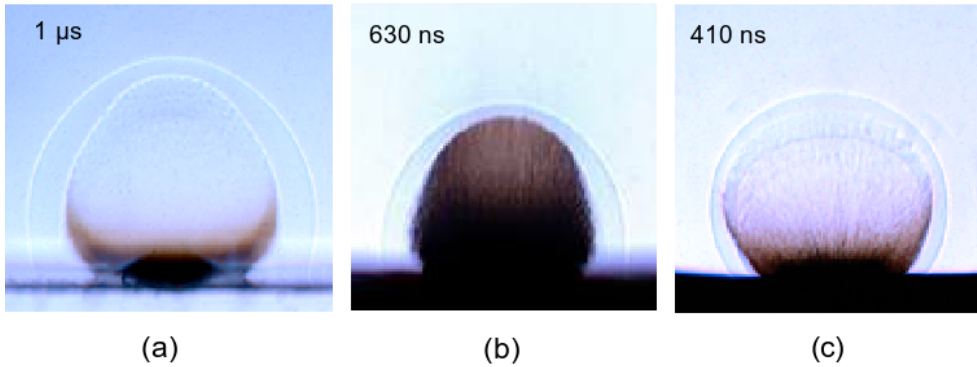


Figure 13. Q-switched Er:YAG laser ablation of (a) water at $\Phi = 1.4 \text{ J/cm}^2$, (b) liver at $\Phi = 1.4 \text{ J/cm}^2$, and (c) liver at $\Phi = 5.4 \text{ J/cm}^2$. The plume consists of water vapour (top) and a droplet/vapour mixture in (a), tissue fragments in (b), and dissociated biomolecules (top) and tissue fragments (bottom) in (c). The volumetric energy densities averaged over the optical penetration depth are $\approx 5.2 \text{ kJ/cm}^3$ in (a), $\approx 4 \text{ kJ/cm}^3$ in (b), and $\approx 9 \text{ kJ/cm}^3$ in (c).

For the ablation of skin at large radiant exposures, a similar sequence of biomolecule dissociation followed by ejection of tissue fragments was observed [37]. However, in this case the ejection of tissue fragments occurred over a shorter time interval than for liver. Ablation ceased when the ablation front reached a depth where the vapour pressure dropped below the tensile strength of the extracellular tissue matrix. Nevertheless, fragment ejection was found to continue for several microseconds after the laser pulse while the tissue matrix is increasingly weakened by thermal denaturation. Generally, the size of the ejected tissue particles is small at early times after the laser pulse and increases with time [37,78]. The entire sequence of phase transitions occurring during water and tissue ablation is summarized in Fig. 14.

Since ablation becomes a volumetric process as soon as the spinodal limit is exceeded and a phase explosion sets in (Sect. 4.4), it is not self-evident why large volumetric energy densities sufficient for a vapour explosion and dissociation of biomolecules should be reached in pulsed laser tissue ablation. However, one needs to consider that the recoil stress produced by the phase transitions of the uppermost tissue layers delays the phase transitions in underlying layers because the spinodal temperature increases with increasing pressure (see Fig. 6). The ongoing absorption of laser energy into the underlying layers can thus drive the thermodynamic state into the supercritical regime. Even larger recoil stresses are produced when these layers are ablated, and the phase transitions in deeper layers are delayed even more. This “positive-feedback” process continues at least until the intensity peak of the laser pulse is reached after which a relaxation process resulting in explosive ablation commences and continues for several microseconds after the end of the laser pulse. The energy densities generated during the runaway process are in the order of 10 kJ cm^{-3} [37] and give rise to recoil pressures of several hundred MPa (Sect. 4.3).

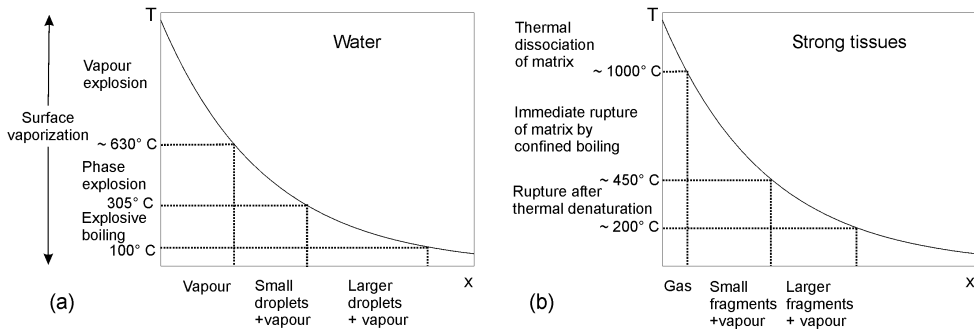


Figure 14. Sequence of phase transitions and corresponding plume constituents in ablation at radiant exposures well above threshold for (a) water ablation, and (b) ablation of mechanically strong tissues such as, for example, skin.

The high volumetric energy density in the target material produced in Q-switched Er:YAG laser ablation results in a very large initial expansion velocity of the ablation plume that drives the emission of an equally fast shock wave. Shock front velocities are usually on the order of 2000–4000 m/s for both IR and UV wavelengths [37, 79–81], i. e., they reach values up to Mach 12. Measured shock wave and plume velocities correlate with the water content of the samples because lower water content results in smaller volumetric energy densities and less vigorous ablation. By contrast, the velocity of particulate fragments is larger for mechanically strong tissues (up to 1700 m/s for skin) than the velocity of droplets ejected in water ablation (up to 280 m/s) [37]. This is because the temperature required for thermal dissociation of the tissue matrix into volatile products is higher than the temperature required for complete vaporization of water. Therefore, tissue fragments become visible early in the ablation process when the ablation front has reached a depth at which the temperature is below the level required for thermolysis. At this time, the pressure driving the ejection is still very high. By contrast, droplet ejection starts only once the temperature at the ablation front has reached a lower level corresponding to the onset of a phase explosion. This results in smaller velocities for the droplet ejection.

The ablation plume exhibits complex dynamics. The plume expansion is nearly spherical during the initial phases of expansion but begins to propagate preferentially in the forward direction after 1–2 μs . For small radiant exposures, the interaction of the piston-like forward movement with the ambient air at rest results in ring vortex formation [37, 82]. For larger radiant exposures, a region of high density and pressure is created at the contact front between plume and surrounding air. The molecules and molecular clusters propagating with the plume possess a non-zero average velocity. When they collide with air molecules that are, on average, at rest, they are partially reflected back into the plume. As visible in Fig. 12, this reflection leads to the formation of an internal shock wave that begins to propagate toward the target surface when the rarefaction from the plume expansion has reduced the

pressure in the plume considerably below its initial value [37,83,84]. The internal shock interacts with the particles and droplets of the plume and deforms the shape of the particle cloud during a time interval lasting about $10 \mu\text{s}$. Due to the heating at the shock front, the passage of the internal shock wave through the reddish droplet cloud results in their vaporization.

The propagation of the shock front after a strong explosion in a homogeneous atmosphere was first theoretically described by Taylor [85] and Sedov [86,87] and, using a higher-order approximation, by Sakurai [88,89]. These theories neglect the mass of the gas and debris driving the shock wave and are thus valid only once the shock wave has swept over a mass of atmospheric gas much greater than the mass in which the energy was initially concentrated. Various authors have later obtained solutions for the mass-dependent flow regime [90–92] and simple analytic solutions are available for some limiting cases. When the mass of the gas encompassed by the shock wave is much greater than the initial ablated mass and the pressure driving the shock is much greater than the atmospheric pressure ahead of the shock front, the position $R(t)$ of a spherical shock wave is governed by [93]

$$R(t) = \xi(E_0/\rho_0)^{1/5} t^{2/5}, \quad (9)$$

and that of a planar shock wave such as emitted from a large irradiated spot size by

$$R(t) = \xi(E_0/\rho_0)^{1/3} t^{2/3}. \quad (10)$$

Here E_0 is the energy driving the explosion, ρ_0 the density of the undisturbed gas, and ξ is a constant that is a function of the specific heat capacity ratio γ of the gas. The peak pressure produced scales proportional to $E_0^{2/5}$. Once the shock wave pressure becomes comparable to the ambient pressure, its propagation is better described by the Jones approximation [94,95]. When the mass of the material removed is very large or the background pressure very low (including vacuum), the motion of a planar shock wave can be described by [96]

$$R(t) = \xi(E_0/\rho_0)^{1/2} t. \quad (11)$$

A comparison of experimental $R(t)$ data with Eqs. (9–11) allows an assessment of the transduction of laser pulse energy into blast wave energy E_0 [95,97].

More refined numerical simulations by Brode [84] and the analytical treatment by Arnold and co-workers [83] include the spherical movements of the external shock front, the contact front between plume and ambient gas, and the internal shock front within the plume. Recently, Chen and co-workers [98] presented a model for the propagation of the external shock wave propagation in atmospheric pressure laser ablation of water-rich targets that incorporates the nonlinear absorption of water and the phase explosion due to superheating. The model predicts a succession of an initially slow plume emission followed by a vigorously accelerated expansion, in good agreement with the experimental results of Apitz and Vogel [37] and with the views presented above.

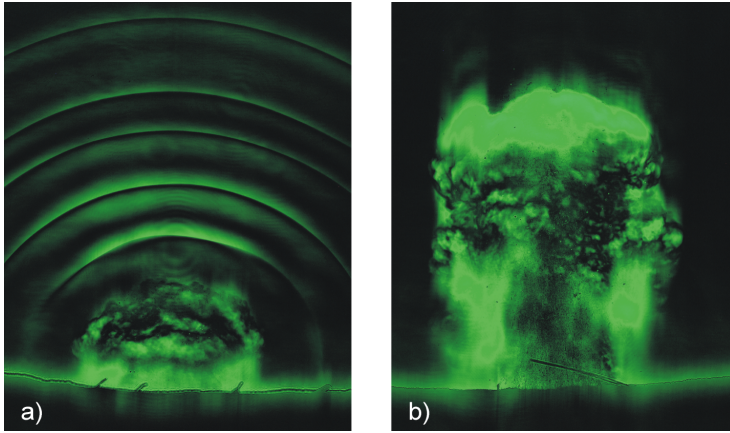


Figure 15. Dark-field Schlieren images of the acoustic transients and ablation plume during skin ablation with a 200- μs Er:YAG laser pulse ($\Phi = 20 \text{ J/cm}^2$, spot size 2.3 mm) photographed (a) 22.4 μs and (b) 40 μs after the onset of the laser pulse. The images show acoustic transients arising from individual spikes in the free-running laser irradiation, and the plume containing vapour and tissue fragments. (Reprinted from Ref. [76] with permission. Copyright 2006 Optical Society of America).

5.2 Primary material ejection in microsecond ablation

Free-running lasers typically provide pulse durations longer than 100 μs . Thus, unlike nanosecond ablation, plume formation and expansion occurs largely during the laser irradiation. As a result, the ablation plume influences the energy deposition of the laser radiation into the tissue target, and the plume dynamics is also influenced by the interaction of the laser beam with the ejected material. Nevertheless, the succession of a sub-ablative phase, development of a vapour plume, and material ejection is similar as with nanosecond pulses even though it occurs on a much longer time scale [99]. However, the heating rates available from microsecond laser pulses are generally much smaller than those available from nanosecond laser pulses of moderate to high radiant exposures. These lower heating rates are not sufficient to generate the temperatures necessary to dissociate ECM molecules and are only able to produce supercritical water at very large radiant exposures.

Free-running laser emission is characterized by intensity fluctuations during the laser pulse (“spiking” behaviour). These intensity peaks modulate the vaporization and material ejection rates [78,100] as well as the emission of acoustic transients generated during the ablation process [101,102]. The intensity spikes of the laser pulse are coupled with the generation of individual transients as shown in Fig. 15.

The mechanisms leading to material ejection are the same as for nanosecond pulses: a phase explosion for mechanically weak materials and a succession of phase explosion and confined boiling for mechanically stronger tissues. Previously it was believed that the generation of a phase explosion requires pulse durations in the nanosecond range [41]. However, using time-resolved photography, Nahen and Vogel [99] demon-

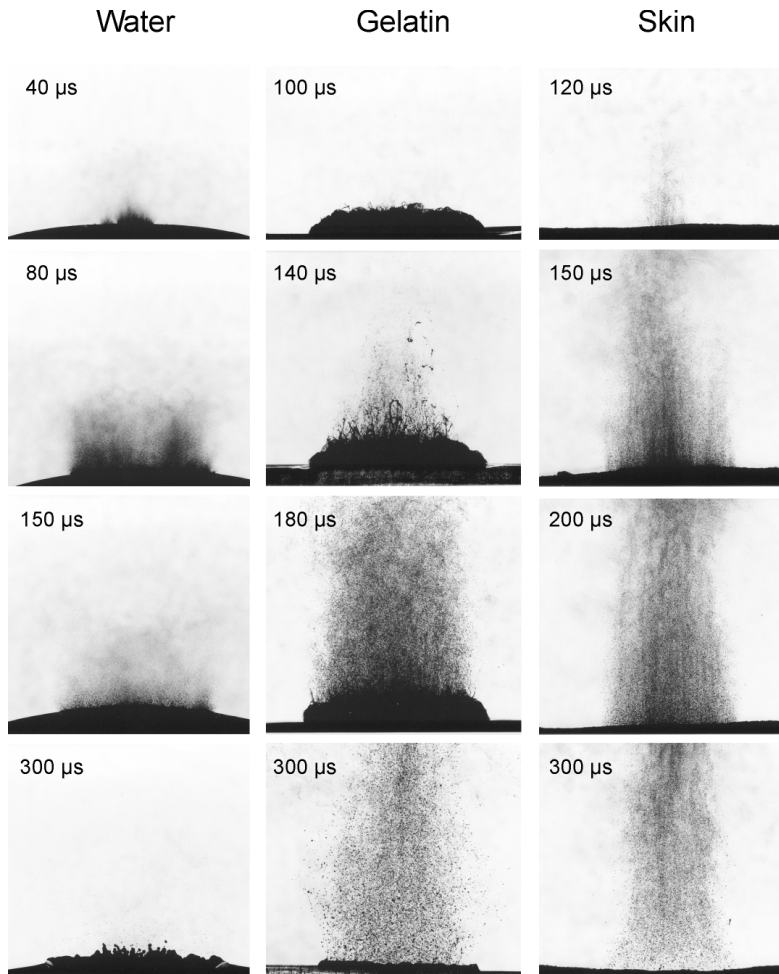


Figure 16. Dynamics of Er:YAG laser ablation of water, gelatin with 70% water content, and skin using a radiant exposure of 4.6 J/cm^2 , 5 mm spot size, and $200 \mu\text{s}$ pulse duration. The times after the beginning of the laser pulse when the photographs were taken are indicated on the individual frames. Note the increasing delay in the ejection of particulate matter with increasing mechanical strength of the target.

strated that a phase explosion can also be produced with pulse durations on the order of $200 \mu\text{s}$. This is shown in Fig. 16 that compares the ablation dynamics for Er:YAG laser irradiation of water, gelatin and skin using identical radiant exposures. The rapid droplet ejection during Er:YAG laser ablation of water can only be produced by a phase explosion because in the absence of stress confinement no other mechanism gives rise to a material ejection perpendicular to the water surface. In gelatin, a phase explosion occurs at the same time as in water. However, the phase explosion only deforms the gelatin surface without rupturing it, and fracture of the

gelatin surface and rapid particle ejection are observed only after a further pressure build-up through confined boiling (Sect. 4.5). The material ejection during skin ablation is also characterized by a phase explosion followed by confined boiling. However, the higher mechanical strength of skin causes a further delay of material ejection compared to gelatin. It is important to note that both for skin and gelatin targets fragments are ejected in the form of solid particles. The absence of droplet-like ejecta indicates that gelatin exposed to temperatures near the spinodal limit does not melt within $200 \mu\text{s}$, even though it melts at 60°C for sufficiently long heat exposures. This finding is consistent with the strong increase in denaturation temperature for very short exposures that was discussed in Sect. 2.

Initial material ejection velocities observed for microsecond laser ablation are roughly one order of magnitude lower than those reported for nanosecond ablation [103]. For free-running pulses, an increase of the radiant exposure results in an earlier onset of the material ejection but does not change the ejection velocity significantly. It is only for very large radiant exposures in which the first intensity spike of the free-running pulse provides a dose in excess of the ablation threshold that an increase of the ejection velocity is observed. By contrast, for nanosecond exposures an increase of the radiant exposure is always coupled with an increase of the volumetric energy density that translates directly into a higher temperature, pressure, and ejection velocity.

In both Q-switched and free-running laser ablation of soft tissues, material ejection continues for a considerable time following laser irradiation that can last up to several milliseconds [78–80,82,99,104]. In general, post-pulse ablation lasts longer for mechanically weaker tissues, larger radiant exposures, and larger laser beam diameters. One possible driving force for the continuation of the ablation process after the end of the laser pulse is the heat retained in the tissue. A progressive weakening of the tissue matrix through thermal denaturation enables a propagation of the ablation front until the vapour pressure in the residual tissue drops below the UTS of the weakened tissue matrix. Another very important source of post-pulse ablation are hydrodynamic phenomena such as recoil stress-induced material expulsion.

5.3 Recoil stress and secondary material ejection

Both the rapidly expanding vapour plume and the ejected particles generate recoil stresses that impart momentum to the tissue. The linear momentum per unit area of the ablated material l is the time integral of the recoil stress σ_{rec} at the target surface

$$l = \int_0^{\infty} \sigma_{\text{rec}}(t) dt. \quad (12)$$

A derivation of the peak recoil stress requires assumptions on the nature and duration of the ablation process. Various authors have presented solutions for the peak stress amplitude produced by a continuous vaporization process [40,66,105,106], and by explosive ablation where the entire laser pulse is deposited prior to the onset of material removal [41,107].

Experimental values for the recoil stress produced by nanosecond laser ablation have been obtained through direct pressure measurements using piezoelectric trans-

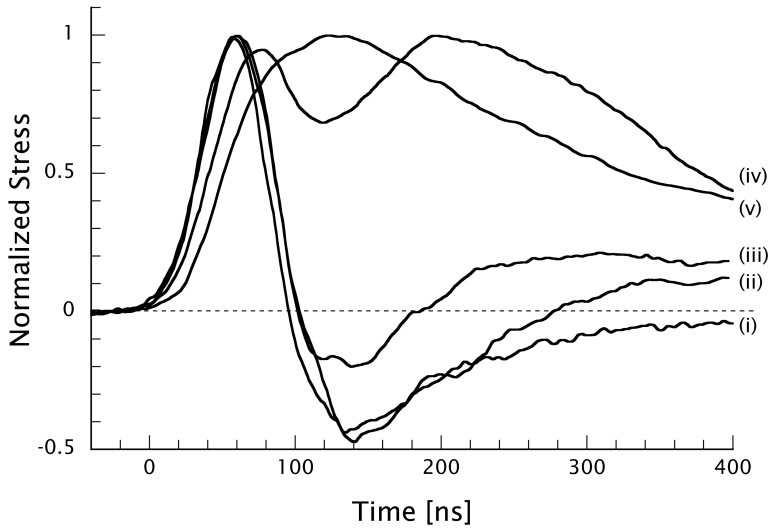


Figure 17. Stress transients resulting from TEA CO₂ laser ($t_p = 30$ ns) irradiation of porcine dermis for radiant exposures below the ablation threshold (i), at threshold (ii), and above threshold (iii)–(v). Radiant exposures below threshold produce bipolar thermoelastic stress transients. For radiant exposures equal to and above threshold, a compressive pulse is produced by the ablative recoil. (Adapted from Ref. [41] with permission. Copyright 1996 Biophysical Society)

ducers [40,41,108,109], and, for water ablation, through analysis of the speed of the recoil-induced shock wave [37]. Peak pressures range from a few MPa at the ablation threshold up to several hundred MPa for radiant exposures well above threshold. For free-running microsecond laser pulses, average stress values during the laser irradiation have been determined through measurement of the recoil momentum using the ballistic pendulum method [65,106], while the peak stress amplitudes produced by the intensity maxima of the free-running pulses were obtained via transducer measurements [109]. Peak values of recoil stress produced during cornea ablation using free-running Er:YSSG laser irradiation at a radiant exposure of 50 J/cm² amounted to 2 MPa [109] while the average pressure value for skin ablation at the same radiant exposure was only 0.3 MPa [106].

In stress-confined tissue ablation, the compressive recoil stress transient is superimposed on a bipolar thermoelastic transient [110]. Figure 17 demonstrates the transition from a bipolar stress transient for radiant exposures below the ablation threshold to a monopolar compressive transient when the ablation threshold is exceeded. This transition and the corresponding increase in peak pressure is a sensitive method for the determination of the ablation threshold [40,41,108].

The recoil stress produced by both vaporization and material ejection in the primary ablation phase can induce a secondary material expulsion process that leads to a strong increase of the ablation efficiency [37,105]. Recoil-induced material expulsion is most pronounced during ablation of liquids and mechanically weak tissues.

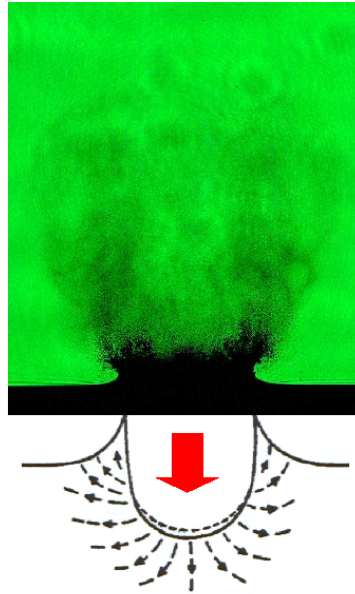


Figure 18. Recoil-induced material expulsion in water ablation by 200- μ s Er:YAG laser pulses, together with a schematic illustration showing the pathlines of the ejected material fragments. The lateral component of the recoil-induced flow collides with the surrounding fluid that is at rest, thus producing an upward directed splash.

Material will be ejected whenever the recoil stress component in the radial direction exceeds the mechanical strength of the tissue, as illustrated in Fig. 18.

The sequence of primary material ejection and recoil-induced material expulsion is shown in Fig. 19 for free-running and Q-switched Er:YAG laser ablation of liver. While the primary material ejection visible at short delay times takes place across the entire ablation area, recoil-induced expulsion occurs preferentially at the ablation crater rim and includes the ejection of tissue fragments much larger than those ejected during the initial phase explosion. The recoil-induced ejection dynamics resembles the surface indentation and subsequent “splash” produced by the impact of liquid droplets on bulk liquids that has already been investigated in considerable detail [111,112]. The mass expelled at later times far exceeds the mass ejected during the primary ablation phase. However, the velocity of the ejecta is considerably slower.

Recoil-induced material expulsion begins after the primary ejection process, requires a radiant exposure well above the ablation threshold, and provides an increase of the ablation efficiency. A marked increase of the ablation efficiency at a certain radiant exposure has been observed for weak tissues as liver and myocardium as well as for gelatin with high water content but not for tissues with greater mechanical strength such as skin [37,113]. Remarkably, no recoil-induced ejection was observed in skin ablation using Q-switched Er:YAG laser pulses even when the recoil stress was about 50 times larger than the quasi-static ultimate tensile strength of skin [37].

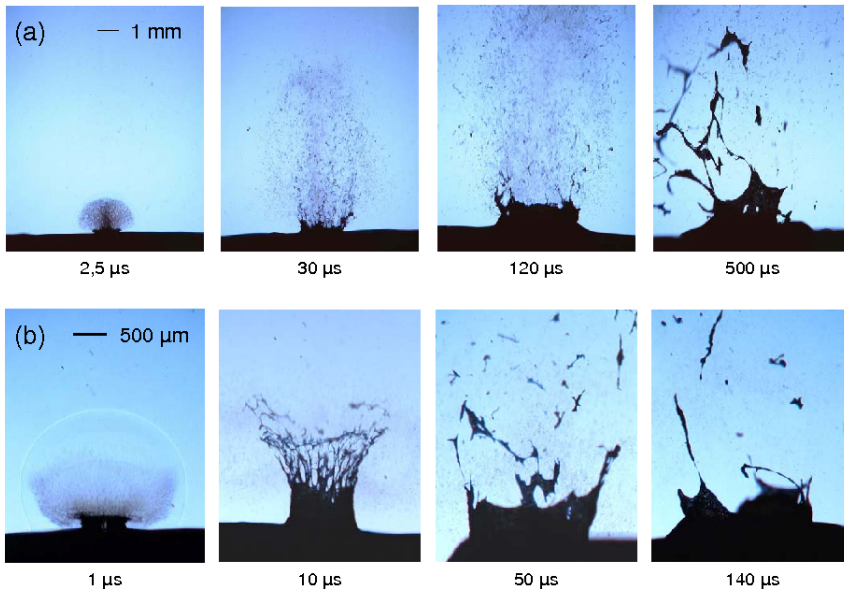


Figure 19. Recoil-induced material expulsion for liver ablation by (a) 200- μs Er:YAG laser pulses at 100 J/cm^2 radiant exposure and 1.1 mm spot size, (b) 70-ns Er:YAG laser pulses at 5.4 J/cm^2 radiant exposure and 0.5 mm spot size. The primary material ejection produced by the phase changes in the target is also visible in all images of (a) and in the first image of (b).

To understand this discrepancy, we must first consider that the recoil-induced tensile and shear stresses that contribute to tissue fracture may be considerably smaller than the measured compressive recoil stress. Moreover, as discussed in Sect. 2, the dynamic tensile strength of tissue at the extreme strain rates produced in pulsed laser ablation is much higher than the quasi-static values for the UTS found in the literature. Finally, tissue fracture will only occur at sufficiently large strain that may not be achieved by stress transients of very short duration [6,22].

For mechanically weak tissues, the recoil-stress-induced material expulsion produces craters with a depth much larger than the optical penetration depth and a diameter much larger than the irradiated spot size, as shown in Fig. 20(a,b). For mechanically strong tissues, the recoil stress does not lead to material expulsion. However, it can produce tissue tearing at the sides of the ablation crater as seen in Fig. 20(c). The cracks and tearing patterns arise preferentially along morphological structures with reduced mechanical strength such as the transitions between corneal lamellae, sinusoid spaces holding blood between plates of cells in liver tissue, and their orientation is also influenced by the weakness of the longitudinal strength of blood vessels compared to their circumferential strength [106]. Tissue tearing at the rim of ablation craters was not observed for skin due to its three-dimensional collagen network that results in an approximately isotropic UTS.

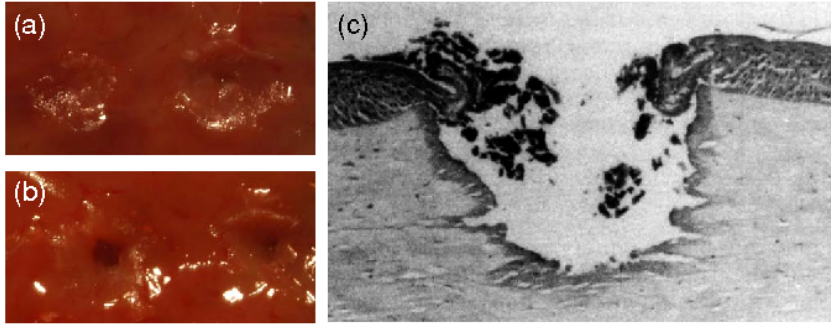


Figure 20. (a,b) Craters produced during liver ablation by 200- μs Er:YAG laser pulses of 32 J/cm^2 and 50 J/cm^2 radiant exposure (2.5 and 1.6 mm spot size, respectively). (c) Histologic slide showing an ablation crater in bovine cornea produced by an Erbium:YSGG laser pulse with $t_p = 250\ \mu\text{s}$ and $\Phi_0 = 100\text{ J/cm}^2$. The tissue around the ablation crater exhibits a 25–50 μm zone of thermal damage (dark) and mechanical tearing between the corneal lamellae. (c) is reprinted from Ref. [106] with permission. Copyright 1993 Optical Society of America).

Recoil-induced stress transients can produce also more subtle forms of collateral tissue damage further away from the irradiation site. Putative photoacoustic damage created during ArF-excimer ($\lambda = 193\text{ nm}$) laser ablation of skin was described by Watanabe and co-workers [114] and Yashima and co-workers [115]. The formation of tensile stress with an amplitude of 3.5 MPa inside the eyeball through diffraction of the recoil stress wave produced during ArF-excimer laser ablation of the cornea was shown by Pini and co-workers [116]. Könz and co-workers [109] demonstrated recoil-induced damage of the corneal endothelium after mid-IR laser ablation of the corneal stroma that was due to the tensile stress generated upon partial reflection of the compressive recoil stress transient at the cornea–aqueous interface.

Thus, to achieve precise and gentle tissue ablation it is not sufficient to simply select a laser wavelength with small optical penetration depth and a pulse duration providing thermal confinement. In addition, one must avoid the production of extensive recoil stresses that may degrade the quality of the ablated surface and/or induce collateral mechanical damage. This restriction imposes an upper limit for the incident radiant exposure.

5.4 Shielding and flow-induced material redeposition

Absorption, scattering, and diffuse reflection of incident laser light by the ablation plume leads to a reduction of the energy delivered to the target tissue and a reduction of the ablation efficiency. Direct measurements of the diffuse reflectance of the plume [117] and of the entire reduction of optical transmission through the plume [99] yielded values of the extinction coefficient within the plume produced by soft tissue ablation using Er:YAG laser irradiation ($\lambda = 2.94\ \mu\text{m}$) on the order of 1 cm^{-1} [99].

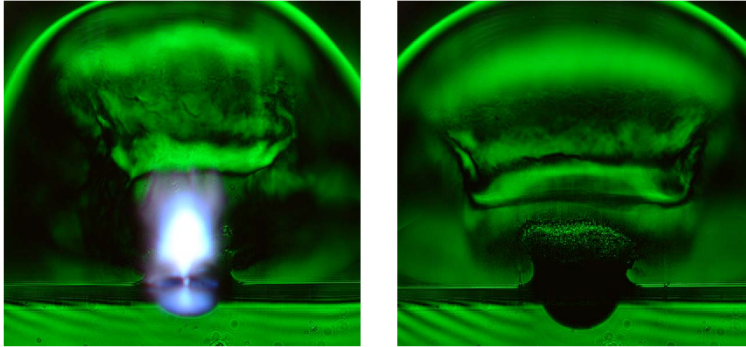


Figure 21. Dark field images of water ablation at $5.4\text{J}/\text{cm}^2$ radiant exposure with and without plasma formation (0.5 mm spot size, image taken $2\mu\text{s}$ after the laser exposure). The plasma originates in hot spots at the water surface and grows into the incoming laser beam. The recoil-induced cavity is considerably smaller in the case with plasma formation due to the “shielding” of the target by light absorption in the plasma. (Reprinted from Ref. [37] with permission. Copyright 2005 Springer Verlag).

Plume reflectance measurements by Nishioka and Domankevitz [117] showed that shielding is strongly enhanced when a series of pulses is applied instead of single pulses. For Er:YAG laser ablation of skin at a spot size of 2 mm, Kaufmann and Hibst observed a decrease of the etch depth per pulse from $40\mu\text{m}$ to $10\mu\text{m}$ when the pulse repetition rate was increased from 1 Hz to 10 Hz [118]. The reduction of the ablation efficiency was attributed to increased shielding by the ablation plume. When a considerably smaller spot size is used, the lateral spread of the plume removes a larger fraction of the ablation products out of the beam path, and the etch depth does not decrease with increasing repetition rate [119].

At very high radiant exposures, plasma formation in front of the target may lead to a further decrease of the optical transmission to the target [37,40,120], as illustrated in Fig. 21. Plasma formation starts at the target surface but the plasma grows rapidly after ignition into the space in front of the target surface causing an effective shielding effect.

When radiant exposures close to the ablation threshold are used, the plume acquires a mushroom-like shape that exhibits a ring vortex at its top, a thin stem with a diameter smaller than the ablation spot and a radial flow component parallel to the surface at the foot of the plume (see also Fig. 12) [37,82,104]. The radial flow parallel to the tissue surface can result in a redistribution of ablation products across the ablation spot. For example, when performing corneal refractive surgery using large laser spot sizes, ablation rates were found to be smaller in the centre of the ablation zone than in its periphery even though the irradiance was spatially homogeneous. As a result “central islands” remained that distorted the intended refractive correction [121]. Photographic investigations of the plume dynamics revealed that the “central islands” are the result of a redeposition of ablated material after the end of the laser pulse that preferentially occurs near the stagnation point of the flow at the

centre of the ablated area [82]. A second factor contributing to the non-uniformity of the ablation rate is the attenuation of subsequent laser pulses in the centre region of the ablated area by remnants of the plume from previous pulses that preferentially stay in the vicinity of the stagnation point [82].

6 Conclusions

6.1 Ablation models

In the previous sections we established that pulsed laser ablation always consists of a sequence of different phase transition processes that occur during and after the laser irradiation. Moreover, we have shown that the initial primary material ejection is often followed by a secondary, recoil-induced, ejection. The type and vigour of the phase transition and ejection processes during an individual ablation event depend on both the laser irradiance and radiant exposure as well as on the optical and mechanical tissue properties. Thus, it is impossible to formulate a simple comprehensive ablation model that describes these different aspects of the ablation process. Nevertheless, it is useful to formulate simplified models that elucidate basic features of the ablation behaviour and parameter dependencies for specific ablation regimes.

One approach is to use metrics of the ablation process such as the threshold, enthalpy, and efficiency of ablation to predict ablation rates without reference to mechanistic aspects of the ablation process. Such heuristic models are particularly valuable to illustrate the ablation behaviour in extreme cases such as the “steady state” model for long laser pulses and the “blow-off” model for very short pulses [6]. Unfortunately, their relative success has, for a long time, obscured the real complexity of the ablation behaviour.

Analytical models that link the ablation outcome to underlying mechanisms provide more insight into the collateral damage arising from ablation than the heuristic models, but all models presented to date are applicable only over a very limited range of radiant exposures and material properties [6]. One will have to resort to computational approaches to model the full complexity of pulsed laser tissue ablation. However, much information on dynamic material properties required for a faithful modelling is still missing. These data include dynamic optical properties (absorption and scattering coefficients), thermal properties (heat capacity, Grüneisen coefficient), and mechanical properties (elastic and shear modulus, ultimate tensile strength) that depend on the magnitude and kinetics of the temperature, pressure, and strain rates achieved during the ablation process. This lack of data is now recognized to be even more important than was thought just a few years ago as recent experimental studies demonstrate that the temperatures and pressures involved in most ablation processes are more extreme than assumed previously. We now know that pulsed laser tissue ablation may be associated with a temperature rise of hundreds to thousands of K, recoil pressures of several hundred MPa, and strain rates on the order of 10^5 to 10^7 s⁻¹ [6,37]. Several of the above mentioned dynamic material properties are presently known only at the lower margin of this parameter space.

Molecular dynamics simulations [122–124] have yielded a wealth of information regarding the inception of phase transitions and the time-evolution of the size and

velocity distribution of the ablation products that are difficult to obtain by other means. However, enormous computational facilities, that are currently unavailable, are required to perform simulations that span the entire spatial and temporal scales usually encountered in realistic applications of tissue ablation.

6.2 Control of ablated mass and thermal and mechanical side effects

The heuristic ablation models mentioned above predict that, if the *removal of large amounts of material* is desired, the use of long laser pulses that achieve a steady-state-like ablation process will be more suitable than ablation based on a blow-off process. This arises because the ablated mass scales linearly with radiant exposure in a steady state ablation process but logarithmically in a blow-off process [6]. However, the difference between the two types of ablation process becomes less pronounced if optical shielding by the ablation products (Sect. 5.4) is significant. A steady state process is most advantageous under conditions where the absorption of the incident laser beam by the ablation plume is markedly smaller than the absorption in the target tissue present in the blow-off situation.

The most direct strategy to *control thermal side effects* involves the selection of a pulse duration that is sufficiently short to minimize heat diffusion during the laser pulse from the volume of energy deposition into the non-ablated tissue (Eq. (4)). However, similar results may also be obtained using longer pulses if the velocity of the ablation front during the laser pulse is comparable or faster than the heat diffusion into the residual tissue. A theoretical analysis of this strategy was presented by Venugopalan and co-workers [53], and experimental evidence for its validity was presented by various authors [53,118,125].

Thermal side effects can be diminished further by selecting laser pulse durations sufficiently short to provide both thermal and stress confinement. Stress confinement serves to lower the ablation threshold and increase the ablation efficiency (Sect. 4.7), and the lowering of the ablation enthalpy in the stress confinement regime reduces the residual heat in the tissue [126,127].

Following the above, high precision ablation can be achieved by selecting a laser wavelength featuring a very small optical penetration depth combined with a short pulse duration sufficient to provide thermal confinement, and, if possible, also stress confinement. However, we showed in Sect. 5.3 that one also needs to avoid the production of extensive recoil stresses to minimize *mechanical side effects*. Extensive recoil stresses may degrade the smoothness of the ablated surface and/or induce collateral mechanical damage; especially in friable tissues [37]. This restriction imposes an upper limit for the incident radiant exposure and implies that the finest tissue effects can be achieved by working close to the ablation threshold.

References

- [1] L. R. Solon, R. Aronson, and G. Gould, 'Physiological implications of laser beams', *Science* **134**, 1506 (1961).
- [2] R. F. Steinert and C. A. Puliafito, *The Nd:YAG Laser in Ophthalmology. Principles and Clinical Practice of Photodisruption* (Saunders, Philadelphia, 1986).
- [3] J. M. Krauss, C. A. Puliafito, and R. F. Steinert, 'Laser interactions with the cornea', *Surv. Ophthalmol.* **31**, 37 (1986).
- [4] A. J. Welch and M. J. C. van Gemert, eds., *Optical-Thermal Response of Laser-Irradiated Tissue* (Plenum Press, New York, 1995).
- [5] M. H. Niemz, *Laser-Tissue Interactions. Fundamentals and Applications* (Springer, Berlin, 2002), 2nd ed.
- [6] A. Vogel and V. Venugopalan, 'Mechanisms of pulsed laser ablation of biological tissues', *Chem. Rev.* **103**, 577 (2003).
- [7] A. Vogel, J. Noack, G. Hüttman, and G. Paltauf, 'Mechanisms of femtosecond laser nanosurgery of cells and tissues', *Appl. Phys. B* **81**, 1015 (2005).
- [8] R. A. J. Eady, I. M. Leigh, and F. M. Pope, 'Anatomy and Organization of Human Skin', in *Rook/Wilkinson/Ebling Textbook of Dermatology*, edited by R. H. Champion, J. L. Burton, D. A. Burns, and S. M. Breathnach (Blackwell Science, Oxford, UK, 1998), 6th ed.
- [9] F. H. Silver, *Biological materials: Structure, Mechanical Properties, and Modeling of Soft Tissue* (New York University Press, New York and London, 1987).
- [10] S. Nomura, A. Hiltner, J. B. Lando, and E. Baer, 'Interaction of water with native collagen', *Biopolymers* **16**, 231 (1977).
- [11] W. F. Cheong, 'Summary of optical properties', in *Optical-Thermal Response of Laser-Irradiated Tissue*, edited by A. J. Welch and M. J. C. van Gemert (Plenum Press, New York, 1995), pp. 275–304.
- [12] R. M. P. Doornbos, R. Lang, M. C. Aalders, F. W. Cross, and H. J. C. M. Sterenberg, 'The determination of in vivo human tissue optical properties and absolute chromophore concentrations using spatially resolved steady-state diffuse reflectance spectroscopy', *Phys. Med. Biol.* **44**, 967 (1999).
- [13] T. L. Troy and S. N. Thennadil, 'Optical properties of human skin in the near infrared wavelength range of 1000 to 2200 nm', *J. Biomed. Opt.* **6**, 167 (2001).
- [14] S. Jacques, 'Role of tissue optics and pulse duration on tissue effects during high-power laser irradiation', *Appl. Opt.* **32**, 2447 (1993).
- [15] S. A. Carp, S. A. Prahl, and V. Venugopalan, 'Radiative transport in the delta-P₁ approximation: accuracy of fluence rate and optical penetration depth predictions in turbid semi-infinite media', *J. Biomed. Optics* **9**, 632 (2004).
- [16] R. Shori, A. A. Walston, O. M. Stafsudd, D. Fried, and J. T. Walsh, 'Quantification and modeling of the dynamic changes in the absorption coefficient of water at 2.94 μm ', *IEEE J. Sel. Topics Quantum Electron.* **7**, 959 (2002).
- [17] J. P. Cummings and J. T. Walsh, 'Erbium laser ablation: The effect of dynamic optical properties', *Appl. Phys. Lett.* **62**, 1988 (1993).
- [18] K. L. Vodopyanov, 'Saturation studies of H₂O and HDO near 3400 cm^{-1} using intense picosecond laser pulses', *J. Chem. Phys.* **94**, 5389 (1991).
- [19] J. T. Walsh and J. P. Cummings, 'Effect of the dynamic optical properties of water on midinfrared laser ablation', *Lasers Surg. Med.* **15**, 295 (1994).
- [20] B. I. Lange, T. Brendel, and G. Hüttmann, 'Temperature dependence of the absorption in water of light at holmium and thulium laser wavelengths', *Appl. Opt.* **41**, 5797 (2002).

-
- [21] P. T. Staveteig and J. T. Walsh, 'Dynamic 193-nm optical properties of water', *Appl. Opt.* **35**, 3392 (1996).
- [22] F. A. Duck, *Physical Properties of Tissue* (Academic Press, London, 1990).
- [23] H. G. Vogel, 'Influence of age, treatment with corticosteroids and strain rate on mechanical properties of rat skin', *Biochim. Biophys. Acta* **286**, 79 (1972).
- [24] R. C. Haut, 'The effects of orientation and location on the strength of dorsal rat skin in high and low speed tensile failure experiments', *Trans. ASME Biomed. Eng.* **111**, 136 (1989).
- [25] G. W. Dombi, R. C. Haut, and W. G. Sullivan, 'Correlation of high-speed tensile strength with collagen content in control and lathyritic rat skin', *J. Surg. Res.* **54**, 21 (1993).
- [26] L. Stryer, *Biochemistry* (WH Freeman and Company, San Francisco, 1987).
- [27] S. Thomsen, 'Pathological analysis of photothermal and photomechanical effects of laser-tissue interactions', *Photochem. Photobiol.* **53**, 825 (1991).
- [28] M. E. Nimni and R. D. Harkness, 'Molecular structure and functions of collagen', in *Collagen. Vol. I Biochemistry*, edited by M. Nimni (CRC Press, Boca Raton, 1988), pp. 1–77.
- [29] J. C. Allain, M. Le Lous, L. Cohen-Solal, S. Bazin, and P. Maroteaux, 'Isometric tensions developed during the hydrothermal swelling of rat skin', *Connect. Tissue Res.* **7**, 127 (1980).
- [30] J. Kampmeier, B. Radt, R. Birngruber, and R. Brinkmann, 'Thermal and biomechanical parameters of porcine cornea', *Cornea* **19**, 355 (2000).
- [31] M. N. Asiyovogel, R. Brinkmann, H. Notbohm, R. Eggers, H. Lubatschowski, H. Laqua, and A. Vogel, 'Histologic analysis of thermal effects of laser thermokeratoplasty and corneal ablation using Sirius-red polarization microscopy', *J. Cataract Refract. Surg.* **23**, 515 (1997).
- [32] M. Le Lous, F. Flandin, D. Herbage, and J. C. Allain, 'Influence of collagen denaturation on the chemorheological properties of skin, assessed by differential scanning calorimetry and hydrothermal isometric tension measurement', *Biochim. Biophys. Acta* **717**, 295 (1982).
- [33] F. C. Henriques, 'Studies of thermal injury. V. The predictability and the significance of thermally induced rate processes leading to irreversible epidermal injury', *Arch. Pathol.* **43**, 489 (1947).
- [34] J. Pearce and S. Thomsen, 'Rate process analysis of thermal damage', in *Optical-Thermal Response of Laser-Irradiated Tissue*, edited by A. J. Welch and M. van Gemert (Plenum Press, New York, 1995), pp. 561–606.
- [35] D. M. Simanowskii, M. A. Mackanos, A. R. Irani, C. E. O'Connell-Rodwell, C. H. Contag, H. A. Schwettman, and D. V. Palanker, 'Cellular tolerance to pulsed hyperthermia', *Phys. Rev. E* **74**, 911 (2005).
- [36] D. M. Harris, D. Fried, L. Reinisch, T. Bell, D. Schlachter, L. From, and J. Burkart, 'Eyelid resurfacing', *Lasers Surg. Med.* **25**, 107 (1999).
- [37] I. Apitz and A. Vogel, 'Material ejection in nanosecond Er:YAG laser ablation of water, liver, and skin', *Appl. Phys. A* **81**, 329 (2005).
- [38] H. S. Carslaw and J. C. Jaeger, *Conduction of Heat in Solids* (Oxford University Press, Oxford, 1959), 2nd ed.
- [39] R. R. Anderson and J. A. Parrish, 'Selective photothermolysis – precise microsurgery by selective absorption of pulsed radiation', *Science* **220**, 524 (1983).
- [40] V. Venugopalan, N. S. Nishioka, and B. B. Mikic, 'The thermodynamic response of soft biological tissues to pulsed ultraviolet laser radiation', *Biophys. J.* **69**, 1259 (1995).
- [41] V. Venugopalan, N. S. Nishioka, and B. B. Mikic, 'Thermodynamic response of soft

- biological tissues to pulsed infrared laser radiation', *Biophys. J.* **70**, 2981 (1996).
- [42] G. Paltauf and P. E. Dyer, 'Photomechanical processes and effects in ablation', *Chem. Rev.* **103**, 487 (2003).
- [43] M. W. Sigrist, 'Laser generation of sound waves in liquids and gases', *J. Appl. Phys.* **60**, R83 (1986).
- [44] J. C. Bushnell and D. J. McCloskey, 'Thermoelastic stress generation in solids', *J. Appl. Phys.* **39**, 5541 (1968).
- [45] G. Paltauf and H. Schmidt-Kloiber, 'Microcavity dynamics during laser-induced spallation of liquids and gels', *Appl. Phys. A* **62**, 303 (1996).
- [46] I. Itzkan, D. Albagli, M. L. Dark, L. T. Perelman, C. von Rosenberg, and M. Feld, 'The thermoelastic basis of short pulsed laser ablation of biological tissue', *Proc. Natl. Acad. Sci. USA* **92**, 1960 (1995).
- [47] G. Paltauf and H. Schmidt-Kloiber, 'Photoacoustic cavitation in spherical and cylindrical absorbers', *Appl. Phys. A* **68**, 525 (1999).
- [48] M. Frenz, G. Paltauf, and H. Schmidt-Kloiber, 'Laser-generated cavitation in absorbing liquid induced by acoustic diffraction', *Phys. Rev. Lett.* **76**, 3546 (1996).
- [49] F. W. Dabby and U. C. Paek, 'High-intensity laser-induced vaporization and explosion of solid material', *IEEE J. Quant. Electron.* **8**, 106 (1972).
- [50] A. Miotello and R. Kelly, 'Critical assessment of thermal models for laser sputtering at high fluences', *Appl. Phys. Lett.* **67**, 3535 (1995).
- [51] R. W. Schrage, *A theoretical study of interphase mass transfer* (Columbia University Press, New York, 1953).
- [52] A. D. Yablon, N. S. Nishioka, B. B. Mikic, and V. Venugopalan, 'Physical mechanisms of pulsed infrared laser ablation of biological tissues', in *Proc. SPIE vol. 3343 - High-Power Laser Ablation*, edited by C. R. Phipps (SPIE, Bellingham, 1998), pp. 69-77.
- [53] V. Venugopalan, N. S. Nishioka, and B. B. Mikic, 'The effect of laser parameters on the zone of thermal injury produced by laser ablation of biological tissue', *Trans. ASME J. Biomech. Eng.* **116**, 62 (1994).
- [54] A. Miotello and R. Kelly, 'Laser-induced phase explosion: New physical problems when a condensed phase approaches the thermodynamic critical temperature', *Appl. Phys. A* **69**, S67 (1999).
- [55] P. Debenedetti, *Metastable Liquids: Concepts and Principles* (Princeton University Press, Princeton, NJ, 1996).
- [56] V. P. Skripov, *Metastable Liquids* (Wiley, New York, 1974).
- [57] V. P. Skripov, E. N. Sinitsyn, P. A. Pavlov, G. V. Ermakov, G. N. Muratov, N. V. Bulanov, and V. G. Baidakov, *Thermophysical properties of liquids in the metastable (superheated) state* (Gordon and Breach Science Publishers, New York, 1988).
- [58] R. E. Apfel, 'Water superheated to 279.5 °C at atmospheric pressure', *Nature Phys. Sci.* **238**, 63 (1972).
- [59] M. M. Martynyuk, 'Phase explosion of a metastable fluid', *Combust. Explos. Shock Waves* **13**, 178 (1977).
- [60] I. I. Frenkel, *Kinetic theory of liquids* (Dover Publications, New York, 1955).
- [61] S. B. Kiselev, 'Kinetic boundary of metastable states in superheated and stretched liquids', *Physica A* **269**, 252 (1999).
- [62] B. Majaron, P. Plestenjak, and M. Lukac, 'Thermo-mechanical laser ablation of soft biological tissue: modelling the micro-explosions', *Appl. Phys. B* **69**, 71 (1999).
- [63] R. M. Verdaasdonk, C. Borst, and M. J. C. van Germert, 'Explosive onset of continuous wave laser tissue ablation', *Phys. Med. Biol.* **35**, 1129 (1990).
- [64] G. L. LeCarpentier, M. Motamedi, L. P. McMath, S. Rastegar, and A. J. Welch, 'Continuous wave laser ablation of tissue: analysis of thermal and mechanical events', *IEEE*

- Trans. Biomed. Eng. **40**, 188 (1993).
- [65] M. Frenz, V. Romano, A. D. Zweig, H. P. Weber, N. I. Chapliev, and A. V. Silenok, 'Instabilities in laser cutting of soft media', J. Appl. Phys. **66**, 4496 (1989).
- [66] A. D. Zweig, 'A thermo-mechanical model for laser ablation', J. Appl. Phys. **70**, 1684 (1991).
- [67] Q. Lu, 'Thermodynamic evolution of phase explosion during high-power nanosecond laser ablation', Phys. Rev. E **67** (2003).
- [68] R. S. Dingus, D. R. Curran, A. A. Oraevsky, and S. L. Jacques, 'Microscopic spallation process and its potential role in laser-tissue ablation', in *Proc. SPIE vol. 2134A - Laser-Tissue Interaction V*, edited by S. L. Jacques (SPIE, Bellingham, 1994), pp. 434-445.
- [69] G. Paltauf and H. Schmidt-Kloiber, 'Model study to investigate the contribution of spallation to pulsed laser ablation of tissue', Lasers Surg. Med. **16**, 277 (1995).
- [70] A. A. Oraevsky, S. L. Jacques, R. O. Esenaliev, and F. K. Tittel, 'Pulsed laser ablation of soft tissue, gels, and aqueous solutions at temperatures below 100°C', Lasers Surg. Med. **18**, 231 (1996).
- [71] G. E. Duvall and G. R. Fowles, 'Shock waves', in *High Pressure Physics and Chemistry*, edited by R. S. Bradley (Academic Press, New York, 1963), pp. 209-291.
- [72] Y. B. Zel'dovich and Y. P. Raizer, *Physics of Shock Waves and High Temperature Hydrodynamic Phenomena*, vol. I and II (Academic Press, New York and London, 1966).
- [73] Q. Lu, S. S. Mao, X. Mao, and R. E. Russo, 'Delayed phase explosion during high-power nanosecond laser ablation of silicon', Appl. Phys. Lett. **80**, 3072 (2002).
- [74] A. Vogel and J. Noack, 'Shock wave energy and acoustic energy dissipation after laser-induced breakdown', in *Proc. SPIE vol. 3254 - Laser-Tissue Interaction IX*, edited by S. L. Jacques (SPIE, Bellingham, 1998), pp. 180-189.
- [75] D. Albagli, L. T. Perelman, G. S. Janes, C. von Rosenberg, I. Itzkan, and M. Feld, 'Inertially confined ablation of biological tissue', Lasers Life Sci. **6**, 55 (1994).
- [76] A. Vogel, I. Apitz, S. Freidank, and R. Dijkink, 'Sensitive high-resolution white-light Schlieren technique with large dynamic range for the investigation of ablation dynamics', Opt. Lett. **31**, 1812 (2006).
- [77] E. Hecht and A. Zajac, *Optics* (Addison Wesley, Reading, MA, 1977).
- [78] J. T. Walsh and T. F. Deutsch, 'Measurement of Er:YAG laser ablation plume dynamics', Appl. Phys. B **52**, 217 (1991).
- [79] Z. Bor, B. Hopp, B. Rácz, G. Szabó, I. Ratkay, I. Süveges, A. Füst, and J. Mohay, 'Plume emission, shock wave and surface wave formation during excimer laser ablation of the cornea', Refract. Corneal Surg. (Suppl.) **9**, S111 (1993).
- [80] J. P. Cummings and J. T. Walsh, 'Q-switched ablation of tissue: plume dynamics and the effect of tissue mechanical properties', in *Proc. SPIE vol. 1646 - Laser-Tissue Interaction III*, edited by S. L. Jacques (SPIE, Bellingham, 1992), pp. 242-253.
- [81] R. R. Krueger and S. L. Trokel, 'Quantitation of corneal ablation by ultraviolet laser light', Arch. Ophthalmol. **103**, 1741 (1985).
- [82] J. Noack, R. Tönnies, C. Hohla, R. Birngruber, and A. Vogel, 'Influence of ablation plume dynamics on the formation of central islands in excimer laser photorefractive keratectomy', Ophthalmology **104**, 823 (1997).
- [83] N. Arnold, J. Gruber, and J. Heitz, 'Spherical expansion of the vapor plume into ambient gas: an analytical model', Appl. Phys. A **69**, S87 (1999).
- [84] H. L. Brode, 'Blast wave from a spherical charge', Phys. Fluids **2**, 217 (1959).
- [85] G. Taylor, 'The formation of a blast wave by a very intense explosion. I Theoretical discussion', Proc. Roy. Soc. A **201**, 159 (1950).

- [86] L. I. Sedov, *Similarity and Dimensional Methods in Mechanics* (Academic Press, New York, 1959).
- [87] L. D. Landau and E. M. Lifschitz, *Fluid Mechanics* (Pergamon Press, Oxford, 1987), 2nd ed.
- [88] A. Sakurai, 'On the propagation and structure of a blast wave, I', *J. Phys. Soc. Japan* **8**, 662 (1953).
- [89] A. Sakurai, 'On the propagation and structure of a blast wave, II', *J. Phys. Soc. Japan* **9**, 256 (1954).
- [90] D. A. Freiwald and R. A. Axford, 'Approximate spherical blast theory including source mass', *J. Appl. Phys.* **46**, 1171 (1975).
- [91] R. Kelly and B. Braren, 'On the direct observation of the gas dynamics of laser-pulse sputtering of polymers. Part I: Analytical considerations', *Appl. Phys. B* **53**, 160 (1991).
- [92] R. Kelly and A. Miotello, 'Pulsed-laser sputtering of atoms and molecules. Part I: Basic solutions for gas-dynamic effects', *Appl. Phys. B* **57**, 145 (1993).
- [93] P. E. Dyer and J. Sidhu, 'Spectroscopic and fast photographic studies of excimer laser polymer ablation', *J. Appl. Phys.* **64**, 4657 (1988).
- [94] D. L. Jones, 'Intermediate strength blast wave', *Phys. Fluids* **11**, 1664 (1968).
- [95] C. Stauter, P. Grard, J. Fontaine, and T. Engel, 'Laser ablation acoustical monitoring', *Appl. Surf. Sci.* **109/110**, 174 (1997).
- [96] D. A. Freiwald, 'Approximate blast wave theory and experimental data for shock trajectories in linear explosive-driven shock tubes', *J. Appl. Phys.* **43**, 2224 (1972).
- [97] C. E. Otis, B. Braren, M. O. Thompson, D. Brunco, and P. M. Goodwin, 'Mechanisms of excimer laser ablation of strongly absorbing systems', in *Proc. SPIE vol. 1856 - Laser Radiation Photophysics*, edited by B. Braren and M. N. Libenson (SPIE, Bellingham, 1993), pp. 132-142.
- [98] Z. Chen, A. Bogaerts, and A. Vertes, 'Phase explosion in atmospheric pressure infrared laser ablation from water-rich targets', *Appl. Phys. Lett.* **89** (2006).
- [99] K. Nahen and A. Vogel, 'Shielding by the ablation plume during Er:YAG Laser ablation', *J. Biomed. Opt.* **7**, 165 (2002).
- [100] K. Nahen and A. Vogel, 'Investigations on acoustic on-line monitoring of IR laser ablation of burned skin', *Lasers Surg. Med.* **25**, 69 (1999).
- [101] K. Nahen and A. Vogel, 'Acoustic signal characteristics during IR laser ablation, and their consequences for acoustic tissue discrimination', in *Proc. SPIE vol. 3914 - Laser-Tissue Interaction XI: Photochemical, Photothermal, and Photomechanical*, edited by D. D. Duncan, J. O. Hollinger D. D. S., and S. L. Jacques (SPIE, Bellingham, 2000), pp. 166-176.
- [102] A. Vogel, B. Kersten, and I. Aplitz, 'Material ejection in free-running Er:YAG laser ablation of water, liver and skin by phase explosion, confined boiling, recoil-induced expulsion and flow-induced suction', in *Proc. SPIE vol. 4961 - Laser-Tissue Interaction XIV*, edited by S. L. Jacques, D. D. Duncan, S. J. Kirkpatrick, and A. Kriete (SPIE, Bellingham, 2003), pp. 40-47.
- [103] R. Hibst, *Technik, Wirkungsweise und medizinische Anwendungen von Holmium- und Erbium-Lasern* (Ecomed, Landsberg, 1996).
- [104] C. A. Puliafito, D. Stern, R. R. Krueger, and E. R. Mandel, 'High-speed photography of excimer laser ablation of the cornea', *Arch. Ophthalmol.* **105**, 1255 (1987).
- [105] D. Bäuerle, *Laser Processing and Chemistry* (Springer, Berlin, 2000).
- [106] J. P. Cummings and J. T. Walsh, 'Tissue tearing caused by pulsed laser-induced ablation pressure', *Appl. Opt.* **32**, 494 (1993).
- [107] C. R. Phipps, R. F. Harrison, T. Shimada, G. W. York, T. P. Turner, X. F. Corlis,

- H. S. Steele, L. C. Haynes, and T. R. King, 'Enhanced vacuum laser-impulse coupling by volume absorption at infrared wavelengths', *Lasers Particle Beams* **8**, 281 (1990).
- [108] P. E. Dyer and R. K. Al-Dhahir, 'Transient photoacoustic studies of laser tissue ablation', in *Proc SPIE vol. 1202 - Laser Tissue Interaction*, edited by S. L. Jacques (SPIE, Bellingham, 1990), pp. 46-60.
- [109] F. Könz, M. Frenz, H. Pratisto, H. P. Weber, H. Lubatschowski, O. Kermani, W. Ertmer, H. J. Altermatt, and T. Schaffner, 'Thermal and mechanical damage of corneal tissue after free-running and Q-switched mid-infrared laser ablation', in *Proc. SPIE vol 2077 - Laser Interaction with Hard and Soft Tissue*, edited by M. J. C. van Gemert, R. W. Steiner, L. O. Svaasand, and H. Albrecht (SPIE, Bellingham, 1994), pp. 78-86.
- [110] R. O. Esenaliev, A. A. Oraevsky, V. S. Letokhov, A. A. Karabutov, and T. V. Malinsky, 'Studies of acoustical and shock waves in the pulsed laser ablation of biotissue', *Lasers in Surg. Med.* **13**, 470 (1993).
- [111] O. G. J. Engel, 'Crater depth in fluid impacts', *J. Appl. Phys.* **37**, 1798 (1966).
- [112] A. Prosperetti and H. N. Oguz, 'The impact of drops on liquid surfaces and the underwater noise of rain', *Annu. Rev. Fluid Mech.* **25**, 577 (1993).
- [113] J. T. Walsh and T. F. Deutsch, 'Er:YAG laser ablation of tissue: Measurement of ablation rates', *Lasers Surg. Med.* **9**, 327 (1989).
- [114] S. Watanabe, T. J. Flotte, D. J. McAuliffe, and S. L. Jacques, 'Putative photoacoustic damage in skin induced by pulsed ArF excimer laser', *J. Invest. Dermatol.* **90**, 761 (1988).
- [115] Y. Yashima, D. J. McAuliffe, S. L. Jacques, and T. J. Flotte, 'Laser-induced photoacoustic injury of skin: effect of inertial confinement', *Lasers Surg. Med.* **11**, 62 (1991).
- [116] R. Pini, F. Rossi, S. Salimbeni, S. Siano, M. Vannini, F. Carones, G. Trabucchi, R. Brancato, and P. G. Gobbi, 'Experimental investigation on acoustic phenomena induced inside the eyeball by excimer laser ablation of the cornea', in *Proc. SPIE vol. 2632 - Lasers in Ophthalmology III*, edited by R. Birngruber and A. F. Fercher (SPIE, Bellingham, 1996), pp. 25-29.
- [117] N. S. Nishioka and Y. Domankevitz, 'Reflectance during pulsed holmium laser irradiation of tissue', *Lasers Surg. Med.* **9**, 375 (1989).
- [118] R. Kaufmann and R. Hibst, 'Pulsed erbium:YAG laser ablation in cutaneous surgery', *Lasers Surg. Med.* **19**, 324 (1996).
- [119] V. Venugopalan, N. S. Nishioka, and B. B. Mikic, 'The effect of CO₂ laser pulse repetition rate on tissue ablation rate and thermal damage', *IEEE Trans Biomed. Eng.* **38**, 1049 (1991).
- [120] J. T. Walsh and T. F. Deutsch, 'Pulsed CO₂ laser tissue ablation: Measurement of the ablation rate', *Lasers Surg. Med.* **8**, 264 (1988).
- [121] J. K. Shimmick, W. B. Telfair, C. R. Munnerlyn, J. D. Bartlett, and S. L. Trokel, 'Corneal ablation profilometry and steep central islands', *J. Refract. Surg.* **13**, 235 (1997).
- [122] L. V. Zhigilei and B. J. Garrison, 'Microscopic mechanisms of laser ablation of organic solids in the thermal and stress confinement irradiation regimes', *J. Appl. Phys.* **88**, 1281 (2000).
- [123] L. V. Zhigilei, E. Leveugle, B. J. Garrison, Y. G. Yingling, and M. I. Zeifman, 'Computer simulations of laser ablation of molecular substrates', *Chem. Rev.* **103**, 321 (2003).
- [124] R. Knochenmuss and L. V. Zhigilei, 'Molecular dynamics model of Ultraviolet matrix-assisted laser desorption/ionization including ionization process', *J. Phys. Chem. B* **109**, 22947 (2005).
- [125] K. T. Schomacker, J. T. Walsh, T. J. Flotte, and T. F. Deutsch, 'Thermal damage

- produced by high-irradiance continuous wave CO₂ laser cutting of tissue', *Lasers Surg. Med.* **10**, 74 (1990).
- [126] M. Frenz, H. Pratisto, F. Könz, E. D. Jansen, A. J. Welch, and H. P. Weber, 'Comparison of the effects of absorption coefficient and pulse duration of 2.12 μm and 2.79 μm radiation on laser ablation of tissue', *IEEE J. Quantum Electron.* **32**, 2025 (1996).
- [127] A. Vogel, P. Schmidt, and B. Flucke, 'Minimization of thermomechanical side effects in IR ablation by use of multiply Q-switched laser pulses', *Med. Laser Appl.* **17**, 15 (2002).